Paleoseismology of Utah, Volume 17

PALEOSEISMIC INVESTIGATION OF THE NORTHERN STRAND OF THE NEPHI SEGMENT OF THE WASATCH FAULT ZONE AT SANTAQUIN, UTAH

by
Christopher B. DuRoss, Greg N. McDonald, and William R. Lund

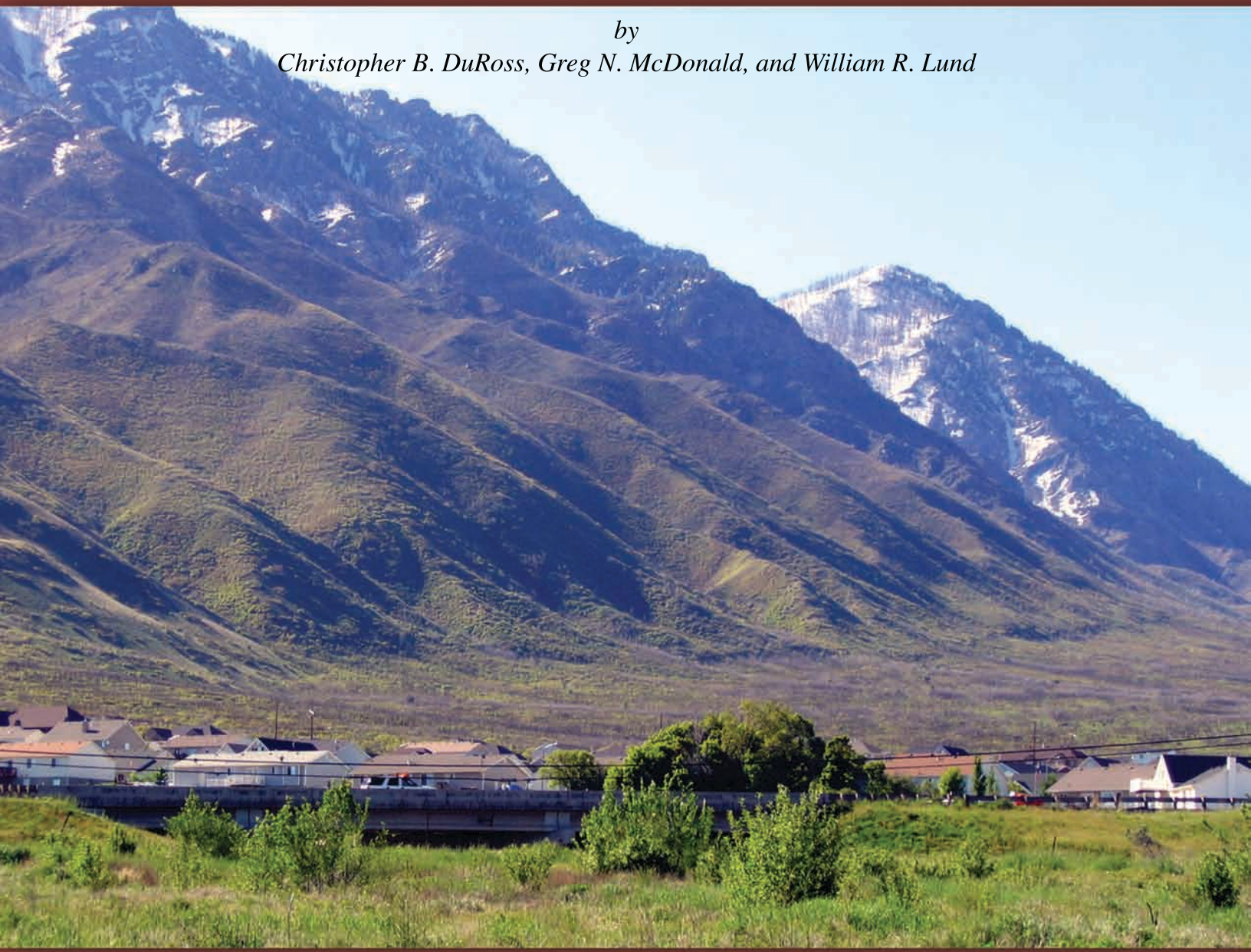

SPECIAL STUDY 124
UTAH GEOLOGICAL SURVEY
a division of
Utah Department of Natural Resources
2008

STATE OF UTAH

Jon Huntsman, Jr., Governor

DEPARTMENT OF NATURAL RESOURCES

Michael Styler, Executive Director

UTAH GEOLOGICAL SURVEY

Richard G. Allis, Director

PUBLICATIONS

contact
Natural Resources Map & Bookstore
1594 W. North Temple
Salt Lake City, Utah 84116
telephone: 801-537-3320
toll free: 1-888-UTAH MAP
Web site: mapstore.utah.gov
email: geostore@utah.gov

UTAH GEOLOGICAL SURVEY

contact
1594 W. North Temple, Suite 3110
Salt Lake City, Utah 84116
telephone: 801-537-3300
fax: 801-537-3400
Web site: geology.utah.gov

CONTENTS

FIGURES

TABLES

PLATE

FOREWORD

This Utah Geological Survey Special Study, *Paleoseismic Investigation of the Northern Strand of the Nephi Segment of the Wasatch Fault Zone at Santaquin, Utah*, is the seventeenth report in the Paleoseismology of Utah series. This series makes the results of paleoseismic investigations in Utah available to geoscientists, engineers, planners, public officials, and the general public. These studies provide critical information regarding paleoearthquake parameters such as earthquake timing, recurrence, displacement, slip rate, and fault geometry and segmentation, which can be used to characterize potential seismic sources and evaluate the long-term seismic hazard of Utah's Quaternary faults.

This report presents the results of a study partially funded through the National Earthquake Hazards Reduction Program to characterize the relative level of activity of the northern strand of the Nephi segment of the Wasatch fault zone (WFZ). The Nephi segment consists of distinct northern and southern strands, and all previous paleoseismic investigations on the segment have been conducted on the southern strand. To resolve issues related to similarities or differences in the timing, displacement, and magnitude of prehistoric surface-faulting earthquakes between the strands, the Utah Geological Survey excavated two trenches on the northern strand at Santaquin while the U.S. Geological Survey simultaneously excavated two trenches at Willow Creek on the southern strand (reported elsewhere). Determining paleoseismic parameters for the entire Nephi segment is important because the new data will help refine segmentation models for the Nephi and Provo segments, which are key components of understanding the past (Holocene) and future behavior of the WFZ, improving WFZ hazard models, and reducing Utah's earthquake-related risk.

Paleoseismic results of this study include determination of the timing and displacement of the most recent surface-faulting earthquake on the northern strand, and estimates of the vertical slip rate and surface-faulting recurrence on the strand.

William R. Lund, Editor
Paleoseismology of Utah Series

Paleoseismology of Utah, Volume 17

PALEOSEISMIC INVESTIGATION OF THE NORTHERN STRAND OF THE NEPHI SEGMENT OF THE WASATCH FAULT ZONE AT SANTAQUIN, UTAH

by

Christopher B. DuRoss, Greg N. McDonald, and William R. Lund

ABSTRACT

As part of ongoing investigations of seismic hazards along the Wasatch Front, the Utah Geological Survey (UGS) has conducted the first paleoseismic investigation of the northern strand of the Nephi segment of the Wasatch fault zone at Santaquin, Utah. The Nephi segment consists of two strands (northern and southern) separated by a 5-km-wide right step. All previous paleoseismic investigations on the Nephi segment have been on the southern strand. To resolve the timing, displacement, and magnitude of prehistoric surface-faulting earthquakes on the Nephi segment, the UGS excavated two trenches across a 3- to 4-m-high fault scarp on the northern strand of the fault near Santaquin, in concert with trenches excavated on the southern strand at Willow Creek by the U.S. Geological Survey. New paleoseismic data resulting from these investigations will also improve fault-segmentation and seismic-hazard models for the Wasatch fault zone as a whole.

The Santaquin trenches show evidence for a single surface-faulting earthquake that displaced early to mid-Holocene alluvial-fan deposits and a fan-surface soil about 3.0 ± 0.2 m down-to-the-northwest. Radiocarbon-dated charcoal fragments separated from the soil on faulted alluvial-fan deposits indicate a maximum time of about 500–550 cal yr B.P. for the most recent surface-faulting earthquake (MRE). Radiocarbon-dated charcoal fragments isolated from an organic horizon contained within colluvium from the MRE indicate a minimum time for the event of about 425 cal yr B.P. Our preferred time for the Santaquin MRE is 500 +100/-150 cal yr B.P., based on these ages and accounting for probabilistic time estimates for the event determined using OxCal radiocarbon calibration and analysis software. A poorly constrained minimum-time estimate for the second earthquake (P2), which was not exposed in the trenches, is at least 1500 cal yr B.P. and likely greater than 6100–7000 cal yr B.P. We could not estimate the recurrence time between the MRE and P2, or a closed-seismic-interval slip rate, but estimated a longer-term geologic vertical slip rate of 0.5 mm/yr using 9 m of displacement across the Bonneville shoreline, which was abandoned at 16,800 cal yr B.P. We determined an average recurrence interval of 6000 ± 400 years by dividing our MRE displacement (2.8–3.2 m) by the longer-term rate. This rate of activity is considerably lower than on the southern strand, and along with disparate late Holocene earthquake chronologies between the strands, suggests that the two strands behave independently.

We estimate a moment magnitude of 7.0 ± 0.3 for the most recent surface-faulting earthquake at the Santaquin site, based on four different fault-parameter versus earthquake-magnitude empirical regressions. The uncertainty in magnitude includes discrepancies between magnitudes determined using surface rupture length (6.5–7.0) and vertical displacement (7.0–7.3). Given our observed 3-m displacement, we estimate that the most recent Santaquin surface-faulting earthquake had a surface rupture length of at least 50 km, which is considerably longer than the length of the northern strand (17 km) and even longer than the entire length of the Nephi segment (42 km). Thus, we consider it unlikely that the Santaquin MRE occurred only on the northern strand as a partial-segment rupture, but rather as (1) part of the rupture of the entire Nephi segment, or (2) part of the MRE rupture on the Provo segment. Our preferred scenario includes the Santaquin MRE as part of a large surface-faulting earthquake on the Provo segment at about 500 cal yr B.P.; however, given differences in the rates of activity on the northern strand and Provo segment, this case of spill-over rupture may be exceptional. Resolving the correct scenario requires comparing the Santaquin MRE parameters with those currently being developed for the Provo segment (Mapleton site; URS Corporation) and southern strand of the Nephi segment (Willow Creek site; U.S. Geological Survey), and with existing paleoseismic information for the Provo, Nephi, and Levan segments.

INRODUCTION

This study presents new information on the timing, displacement, and magnitude of the most recent surface-faulting earthquake (MRE) on the northern strand (figure 1) of the Nephi segment of the Wasatch fault zone (WFZ). The new paleoseismic data are derived from two fault trenches on the northern strand excavated in the spring of 2005 by the Utah Geological Survey (UGS) east of Santaquin, Utah (figure 2). The Santaquin trench study is part of a cooperative research project between the UGS and U.S. Geological Survey (USGS), which was partially funded by the USGS's National Earthquake Hazards Reduction Program. The USGS (Machette and others, 2007) excavated fault trenches on the southern strand of the Nephi segment near Willow Creek, east of Mona, Utah, about 20 km south-southwest of the Santaquin site (figure 1). The purpose of the cooperative investigations is to resolve discrepancies in the paleoseismic his-

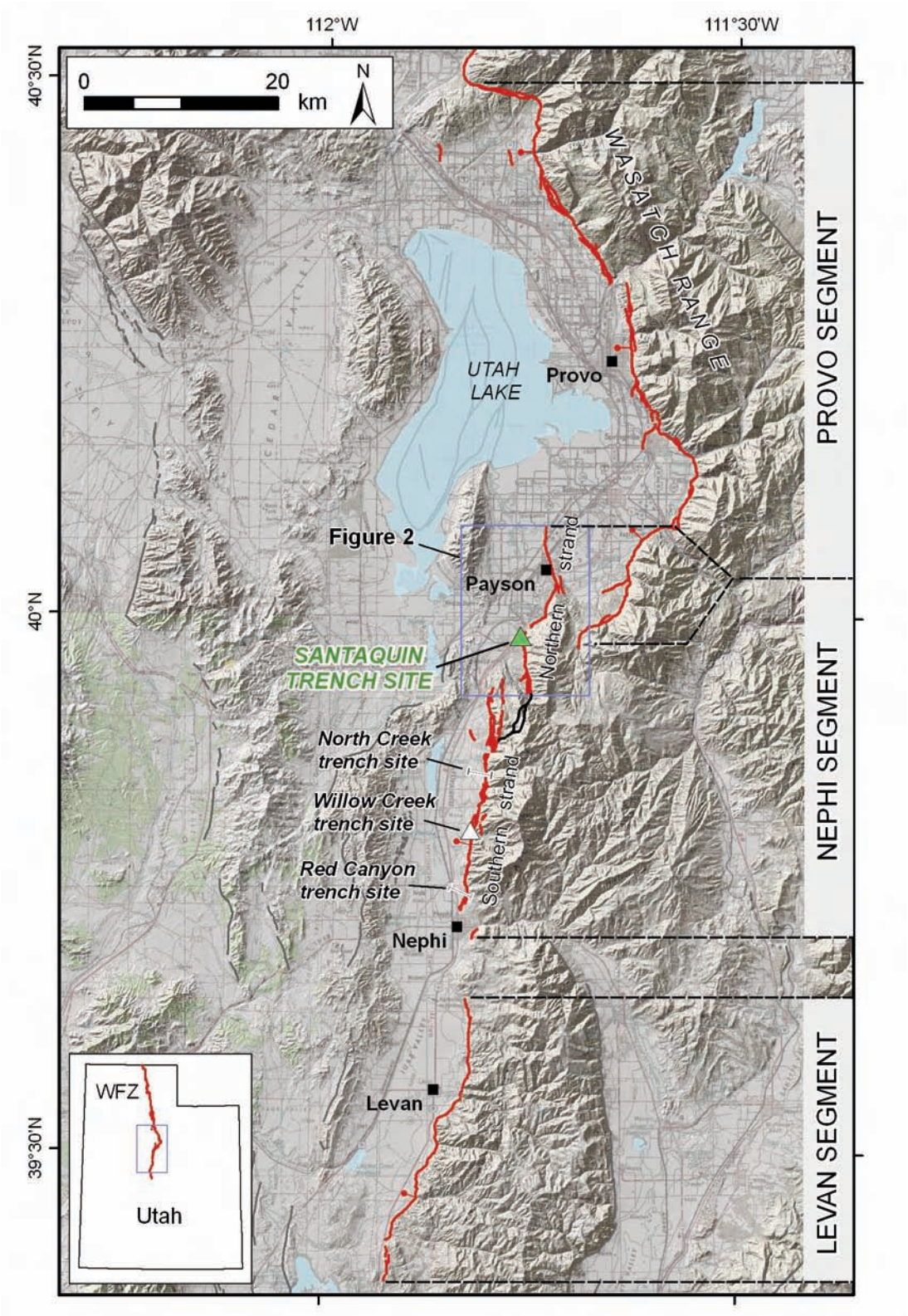

Figure 1. *Surface trace of the Provo, Nephi, and Levan segments of the Wasatch fault zone (WFZ; inset) showing northern and southern strands of the Nephi segment, and locations of the Santaquin trench site, Willow Creek trench site (USGS), and pre-2005 trench sites (I shapes). Trace of WFZ (red) and other Quaternary faults (gray) from Black and others (2003); ball and bar on downthrown side. Cross fault (black) between northern and southern strands of Nephi segment modified from Harty and others (1997) and DuRoss (unpublished data, 2004). Blue box is area of figure 2. Basemaps: scanned USGS 1:250,000-scale topographic map and 30-m digital elevation model.*

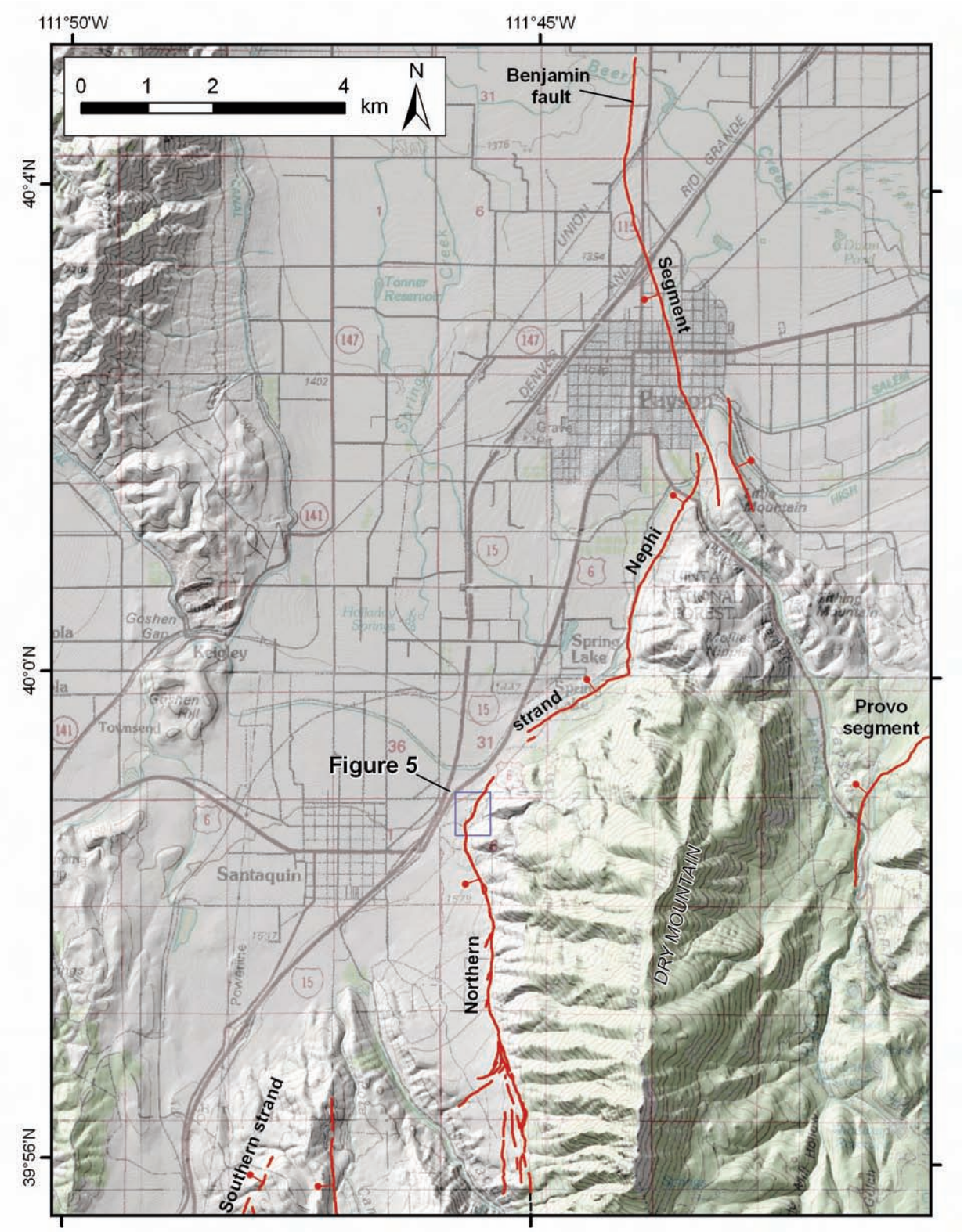

Figure 2. *Northern strand of the Nephi segment. Fault traces from Machette (1992), Harty and others (1997), and Black and others (2003); ball and bar on downthrown side of faults. Blue box is area of figure 5. Basemaps: scanned USGS 1:100,000-scale topographic quadrangle and 10-m digital elevation model.*

tory of the Nephi segment, and to accurately characterize its seismic potential by determining the frequency and size of Holocene surface-faulting paleoearthquakes on both the northern and southern strands. This report presents the results of the UGS's investigation at the Santaquin trench site.

The new paleoseismic data resulting from the cooperative studies will also be used to improve our understanding of the overall behavior of the WFZ. For example, comparing Nephi-segment earthquake parameters (e.g., timing, displacement, and magnitude) and rates of fault slip with those for the adjacent Provo and Levan segments (figure 1) will help refine fault-segmentation and seismic-hazard models for the WFZ. Ultimately, the paleoearthquake information is critical to accurately portray the hazards associated with the WFZ, and will aid in improving our knowledge of strain accumulation and release during large-magnitude surface-faulting earthquakes along segments of the WFZ.

Geologic Setting

Wasatch Fault Zone

The 343-km-long WFZ extends along the western base of the Wasatch Range, which forms the eastern physiographic boundary of the Basin and Range Province (BRP) in north-central Utah (figure 3). The WFZ poses a significant earthquake hazard to Utah's heavily urbanized Wasatch Front, and also is important in understanding spatial and temporal trends of surface-faulting earthquakes in the BRP. The WFZ accommodates east-west extension in the BRP (figure 3), and has been shown to release strain in large-magnitude (M 6.7–7.3; table 1) surface-faulting earthquakes along quasi-independent seismogenic fault segments (Swan and others, 1980; Schwartz and Coppersmith, 1984). Ten segments have been delineated using structural, geological, geophysical, and seismological data (Machette and others, 1992; figure 3). Variations in the Holocene paleoseismic history and geometry of Quaternary fault traces also provide the basis for segmentation models for the central six segments from near Brigham City to Levan (Swan and others, 1980; Schwartz and Coppersmith, 1984; Machette and others, 1992; Lund, 2005). The central WFZ segments are similar in trace length, displacement, orientation, and morphology to BRP faults that have produced historical, large-magnitude surface-faulting earthquakes (table 1). Recent advancements in understanding the paleoearthquake behavior of the central WFZ include refinements of longer-term (latest Pleistocene to present) paleoseismic records (e.g., McCalpin, 2002; McCalpin and Forman, 2002; Olig and others, 2004) and investigations into the potential for partial-segment, spill-over, and multiple-segment rupture along the fault (e.g., Chang and Smith, 2002; DuRoss, 2006; Nelson and others, 2006).

The five central segments of the WFZ from Brigham City to Nephi (figure 3) each has evidence for multiple surface-faulting earthquakes in the past 6000 years. The average recurrence time for Holocene surface faulting on an individual segment ranges from 1300 to 2500 years (Lund, 2005), and is 350–400 years for all five segments combined (Machette and others, 1992; McCalpin and Nishenko, 1996). The segments range from 36 to 59 km long (straight-line distance, table 1; Machette and others, 1992; Black and others, 2003), have vertical displacements per surface-faulting earthquake ranging from about 1 to 4 m (table 1), and have Holocene vertical slip rates of about 1.1 to 1.4 mm/yr (Lund, 2005). The contemporary rate of horizontal extension across the central WFZ is 1.6 ± 0.4 mm/yr based on campaign (1992–2003) and continuous (1997–2004) global positioning satellite (GPS) data, assuming spatially homogeneous strain within a 65-km-wide zone extending from near Brigham City to Nephi (Chang and others, 2006). Of the five central WFZ segments, the Nephi segment has had the least well constrained record of repeated, frequent Holocene faulting (Lund, 2005). The poor record stems from conflicting results from early paleoseismic investigations and a lack of continued study due to its distance from the heavily urbanized areas of the southern Wasatch Front and a location mostly within the Mount Nebo Wilderness study area.

Nephi Segment

The Nephi segment extends 42 km from Nephi to north of Payson, and has evidence for late Quaternary surface faulting along two distinct strands: the 17-km-long northern strand and 25-km-long southern strand (Machette and others, 1992; DuRoss and Bruhn, 2005) (figures 1 and 2). The northern strand bounds the west side of Dry Mountain and the southern strand bounds the west side of the Wasatch Range east of Juab Valley; a 5-km-wide right step separates the two strands (figure 2). A 6-km-long, northeast-striking cross fault connects the southern and northern strands (figure 1; Machette and others, 1992; Harty and others, 1997; DuRoss, 2004). DuRoss (2004) found no evidence of Holocene or late Pleistocene displacement along the cross fault, but heavy vegetation and landslides may obscure late Quaternary displacement. The Nephi segment is separated from the Provo segment to the north by a 4.5- to 9-km-wide overlapping right step (Payson salient), and from the Levan segment to the south by a 15-km gap in Holocene and latest Pleistocene surface faulting (figure 1; Hylland and Machette, 2004; Hylland and Machette, in press).

Surficial deposits along the Nephi segment include middle Pleistocene to late Holocene alluvial-fan deposits sourced from drainages in the Wasatch Range, and lacustrine deposits related to late Pleistocene Lake Bonneville (Harty and others, 1997). The Lake Bonneville highstand shoreline was abandoned at 16,800 cal yr B.P. (calendar years before present [A.D. 1950]) (D.R. Currey, University of Utah, written communication to UGS, 1996; see also Lund, 2005, table 4). This shoreline is poorly expressed on the southern strand but well expressed along parts of the northern strand. Other surficial deposits include landslides, rock falls, hillslope colluvium, and debris flows (Machette, 1992; Harty and others, 1997). Precambrian metamorphic rocks, and faulted and folded Paleozoic to Cenozoic sedimentary and volcanic rocks are exposed in the footwall block of the WFZ (Witkind and Weiss, 2002; Felger and others, 2004).

Previous Investigations

Trenching

Prior to this study, paleoseismic data for the Nephi segment were limited to the southern strand, and poorly con-

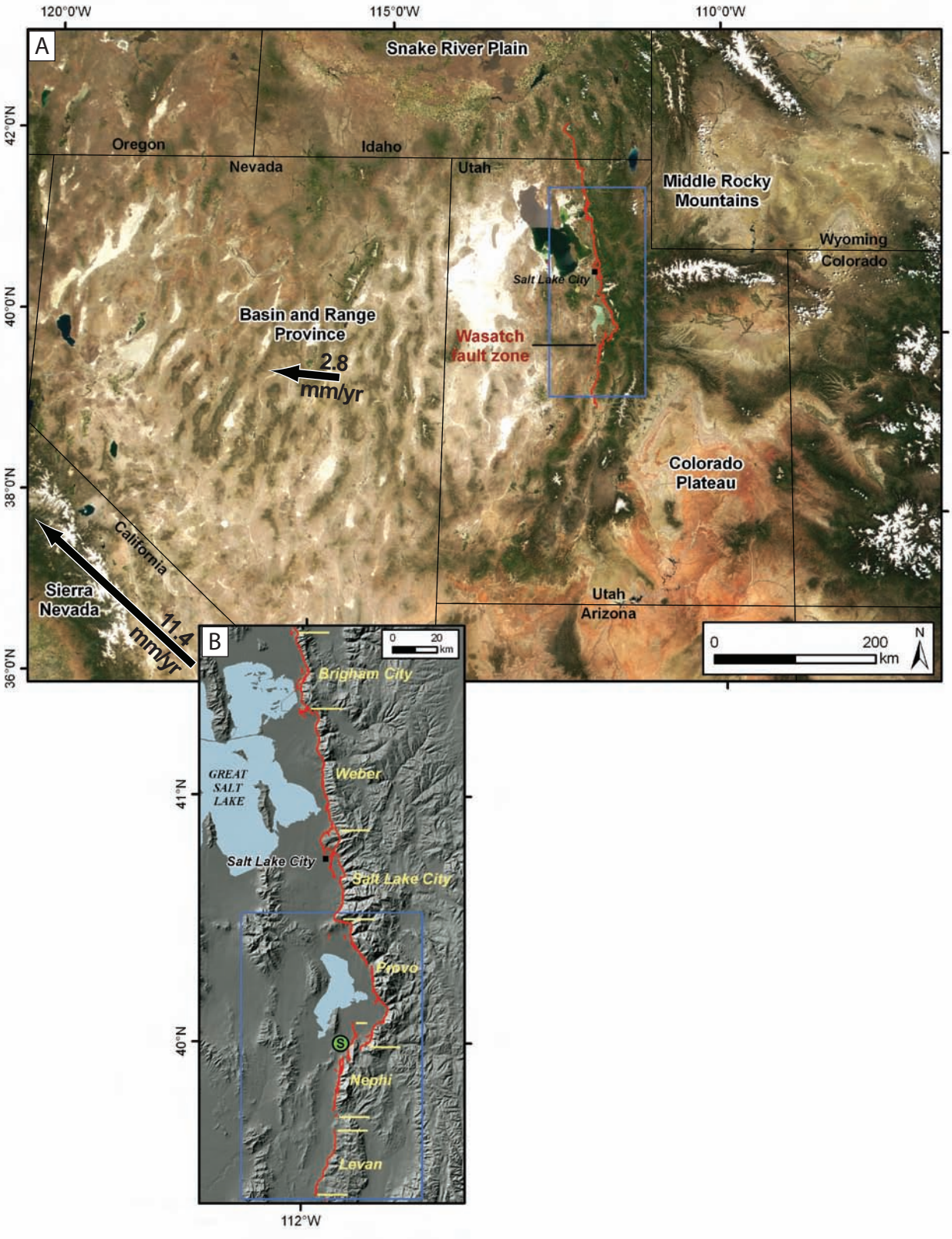

Figure 3. *(A) Physiographic provinces of Utah and surrounding states. Arrows indicate approximate geodetic motion vectors and rates of the central Basin and Range Province and Sierra Nevada - Great Valley areas relative to the Colorado Plateau (modified from Bennett and others, 2003). Blue box is area of figure 3B. True-color satellite image of Utah and Nevada from National Aeronautics & Space Administration (NASA, 2006), taken May 31, 2001. (B) Central segments of the WFZ. Horizontal yellow lines indicate segment boundaries. S indicates location of the Santaquin trench site. Blue box is area of figure 1.*

***Table 1**. Selected parameters for Basin and Range Province earthquakes and WFZ segments.*

Fault/fault segment[1]	SRL[2] (km)	Vertical displacement[3] (m)				Magnitude[4]		
		P1	P2	P3	P4	M_S	M_W^{SRL}	M_W^{VD}
Prehistoric (WFZ)								
Brigham City segment, WFZ	36	0.5-1.3	1.0–1.1	1.5–2.5	0.9–2.5	7.2	6.9	7.0 [2.5 m]
Weber segment, WFZ	56	0.5–2.6*	2.3–4.2	0.9–4.2	1.4	7.3	7.1	7.2 [4.2 m]
Salt Lake City segment, WFZ	39	1.5–2.5	1.5–2.5	1.5–2.5	-	7.2	6.9	7.0 [2.5 m]
Provo segment, WFZ	59	1.4–3.3	2.2–2.7	2.2–2.7	-	7.3	7.1	7.1 [3.3 m]
Nephi segment, WFZ	42	1.1–2.2	1.3–2.5	1.4–2.0	-	7.2	7.0	7.0 [2.5 m]
Levan segment, WFZ	26	1.8–3.0	-	-	-	7.1	6.7	7.0 [3.0 m]
Historical (BRP) earthquakes	**SRL (km)[2]**	**D (m)**				M_S	M_W^{SRL}	M_W^{VD}
1915 Pleasant Valley, Nevada	59	5.8				7.6	7.1	7.3
1954 Dixie Valley, Nevada	45	3.8				6.8	7.0	7.1
1954 Fairview Peak, Nevada	67	4.8				7.2	7.2	7.2
1959 Hebgen Lake, Montana	28	5.5				7.5	6.7	7.3
1983 Borah Peak, Idaho	34	2.7				7.3	6.9	7.0

[1] WFZ – Wasatch fault zone, BRP – Basin and Range Province; earthquakes of M >6.5 (dePolo and others, 1991; McCalpin, 1996).

[2] SRL – surface rupture length (straight-line distance). Prehistoric SRL from Machette and others (1992), Black and others (2003), and Lund (2005); historical SRL from Wells and Coppersmith (1994).

[3] Wasatch fault vertical displacement based on existing fault trench data (Lund, 2005); values reported as minimum-maximum displacement ranges; P1, P2, P3, and P4 are paleoearthquakes (P1 = most recent event (MRE). *The Weber segment MRE net displacement is based on events D (0.5–0.8 m) and C (1.7–2.6 m) of Nelson and others (2006) (events Za and Zb, respectively, of Lund, 2005). Historical earthquake displacements (D) from compilation by Wells and Coppersmith (1994) except Hebgen Lake earthquake displacement, which is from Schwartz (2000); values are maxima.

[4] M_S is surface-wave magnitude (prehistoric M_S based on SRL [Bolt, 1999]; historical M_S from Wells and Coppersmith, 1994); M_W^{SRL} is moment magnitude based on all-fault-type SRL regression in Wells and Coppersmith (1994); M_W^{VD} is moment magnitude based on inferred maximum displacement (number in brackets is value used in calculation), using all-fault-type regression in Wells and Coppersmith (1994).

strained the segment's Holocene earthquake history. Previous paleoseismic investigations included trench excavations at North Creek (Hanson and others, 1981) and Red Canyon (Jackson, 1991) (figure 1), which together identified three surface-faulting earthquakes since the middle Holocene on the basis of fan alluvium radiocarbon dated by Bucknam (1978) at 4500 and 5200 cal yr B.P. (4000 ± 400 and 4580 ± 250 ^{14}C yr B.P., respectively; table 2). However, these early investigations produced conflicting sets of numerical ages, and as a result, significantly different earthquake chronologies are possible depending on how the age determinations are treated.

Age determinations: To treat the existing age data in a consistent manner, we compiled all thermoluminescence and radiocarbon ages published by Hanson and others (1981, 1982a, 1982b) and Jackson (1991) and corrected the ^{14}C ages following the method of Nelson and others (2006) (table 2). We did not calendar calibrate radiocarbon ages on bulk-soil organics (apparent mean residence time [AMRT] ages; see Machette and others, 1992), but rather, for each sample we applied a single calendar correction to the mean ^{14}C age equal to the deviation from the solar calendar, if greater than 150 years. We also corrected the AMRT ages for an inferred inherited age of 300 ± 200 years at the time of burial (mean-residence-time [MRT] correction) by subtracting 500 years from the lower (younger) end and 100 years from the upper (older) end of the two-sigma, calendar-corrected age range (after Nelson and others, 2006). For example, for North Creek AMRT sample WC-12-80-7a (Hanson and others, 1981), we corrected the ^{14}C age of 3640 ± 75 ^{14}C yr B.P. by applying a calendar correction of +350 years (determined by subtracting the mean ^{14}C age from the midpoint of the two-sigma calendar-corrected age range). The calendar-corrected age is then the ^{14}C mean age (3640 ^{14}C yr B.P.) plus the calendar correction (350 years) with an uncertainty equal to the doubled lab uncertainty, resulting in a calendar-corrected two-sigma age of 3800–4100 cal yr B.P. We then applied an MRT correction of 300 ± 200 years to this age, yielding an estimated time of soil burial of 3300–4000 (midpoint of 3700; rounded to the nearest century) cal yr B.P. Similar results are obtained by using a calendar-calibration program to correct the AMRT ^{14}C ages (method of Machette and others, 1992). However, we prefer the method of Nelson and others (2006) because (1) calendar-correction procedures are designed for specific ^{14}C ages, rather than ages resulting from dating various soil fractions, and (2) the broader age ranges obtained are more suitable given uncertainties in relating bulk-soil ages to earthquake timing.

For charcoal samples, we calendar calibrated the ^{14}C ages using the CALIB 5.0 calibration program (Stuiver and Reimer, 1993) and the non-marine calibration dataset IntCal04 (Reimer and others, 2004). We did not apply a laboratory uncertainty multiplier or specify a sample age span (i.e., an estimated elapsed time for sample growth or formation; Stuiver and others, 2005). Ages are reported as the midpoint of the calendar-calibrated, two-sigma range, rounded to the nearest century. For example, for North Creek charcoal sample WC-12-80-6 (1110 ± 60 ^{14}C yr B.P.), the two-sigma, calendar-corrected age range is 900–1200 cal yr B.P., with a midpoint of 1100 cal yr B.P. (table 2).

North Creek site: At North Creek, Hanson and others (1981) excavated three trenches, which exposed stratigraphic evidence for two surface-faulting earthquakes. The more recent paleoearthquake (P1) displaced alluvial-fan deposits containing organic-rich soils and charcoal. Charcoal recovered from soils formed both within faulted alluvial-fan sediments and on possible older scarp colluvium yielded ages of 400 cal yr B.P. (300 ± 300 ^{14}C yr B.P.; table 2) for one sample and 1100 cal yr B.P. (1110 ± 60 ^{14}C yr B.P.; table 2) and 800 cal yr B.P. (700 ± 250 ^{14}C yr B.P.; table 2) for a second sample (figure 4). Detrital charcoal collected from the faulted alluvial-fan deposits yielded ages of 1300 cal yr B.P. (1350 ± 70 ^{14}C yr B.P.; table 2) and 1600 cal yr B.P. (1550 ± 300 ^{14}C yr B.P.; table 2) for one sample and 1200 cal yr B.P. (1200 ± 300 ^{14}C yr B.P.; table 2) for a second sample. All six ages are from the faulted alluvial-fan and colluvial units, charcoal entrained in them, and soils developed on them and thus provide a maximum-limiting time constraint for P1 (figure 4). However, based on the steep scarp angles at North Creek and the presence of a knickpoint in a stream channel just above the scarp, Hanson and others (1982b) and Schwartz and Coppersmith (1984) preferred a P1 time of about 300–500 years. Radiocarbon-dated charcoal collected from within a post-faulting, historical debris flow provide minimum-limiting time constraints for P1 of about 300 and 400 cal yr B.P. (0 ± 300 and 250 ± 300 ^{14}C yr, respectively; table 2, figure 4); however, no discussion or further justification of these ages was given by Hanson and others (1981, 1982a, 1982b).

The timing of a second paleoearthquake (P2) is constrained by seven radiocarbon ages from one charcoal and four bulk-soil samples (one sample yielded one conventional and two AMS ages) collected from a soil formed on top of the P2 colluvial wedge (table 2, figure 4). Since the scarp colluvium (and soil developed on it) formed after the time of P2, the ages provide a minimum-limiting time constraint for P2. The ages cluster in two groups: one group (four ages) between 1300 and 1400 cal yr B.P. (1389 +181/-177, 1645 +270/-262, 1650 ± 50, and 1700 ± 300 ^{14}C yr B.P.; table 2), and a second group (three ages) between 3700 and 4100 cal yr B.P. (3640 ± 75, 3850 ± 400, and 3894 +288/-278 ^{14}C yr; table 2). Hanson and others (1982a, 1982b) considered that the younger ages "may represent younger material incorporated into the soil prior to burial," and interpreted the older set of ages as representative of the soil and therefore providing a minimum limit of 3700–4100 years on the timing of P2.

Hanson and others (1981) inferred a third paleo-earthquake (P3) from an inset stream terrace in the upthrown block. That earthquake must have occurred after 5200 or 4500 cal yr B.P., based on conventional and AMS radiocarbon ages, respectively, from charcoal collected by Bucknam (1978) from a natural exposure of North Creek alluvial-fan deposits east of the fault (figure 4). Hanson and others (1981) also reported a radiocarbon age (sample WC-12-80-3; table 2) for a soil developed on "North Creek alluvium" exposed in a test pit on the downthrown side of the fault, but the sample location and its relation to surface faulting are uncertain.

Red Canyon site: At the Red Canyon trench site, 12 km south of North Creek and close to the southern termination of surface faulting on the Nephi segment (figure 1), Jackson (1991) cited three stacked, fault-scarp-derived colluvial wedges as evidence for repeated Holocene surface faulting. Timing of P1 is constrained by an age of 2800 cal yr B.P. (2900 ± 90 ^{14}C yr B.P.; table 2) and a thermoluminescence (TL) age of 1300 ± 500 cal yr B.P. (table 2) for a thin, weak soil on P2 colluvium buried by a block of alluvial-fan strata within P1 colluvium. A second TL age for a similar soil buried by the P1 colluvial wedge about 4 m west of the main fault is 1500 ± 400 cal yr B.P (table 2). Jackson disregarded the 2800-yr ^{14}C age, and used the two closely corresponding TL ages to assign a timing of about 1400 cal yr B.P. to P1.

To investigate P2 timing, Jackson (1991) sampled and dated a soil buried by P2 colluvium. Jackson (1991) obtained one set of ^{14}C and TL ages on bulk organics from a soil developed on the P3 colluvial wedge and buried by the P2 colluvial wedge adjacent to the main fault zone, and a second set of ^{14}C and TL ages on bulk organics where a correlative soil is buried by P2 colluvium about 3.5 m west of the main fault. The first set includes a ^{14}C age of 1100 cal yr B.P. (1380 ± 120 ^{14}C yr B.P.) and TL age of 1700 ± 200 cal yr B.P., both of which Jackson considered too young. The second set of ages includes a radiocarbon age of 3800 cal yr B.P. (3690 ± 170 ^{14}C yr B.P.; table 2) and TL age of 7000 ± 800 cal yr B.P (table 2). Jackson considered the TL age too old, and after applying a large MRT correction to the radiocarbon age of 3800 cal yr B.P., concluded that P2 occurred between 3000 and 3500 cal yr B.P., which corresponded reasonably well with the North Creek P2 timing of greater than about 3700 cal yr B.P.

The minimum time since P3 at Red Canyon is constrained by an age of 3600 cal yr B.P. (3550 ± 150 ^{14}C yr B.P.; table 2) on bulk organics collected from the base of the P3 colluvial wedge. Jackson used this age and the 3800-year age for the soil developed on the P3 wedge to interpret P3 as having occurred before 3900 cal yr B.P., but after deposition of 7–15 ka alluvial-fan sediments (samples ITL-90 and ITL-48; table 2) it displaces. However, considering the Bucknam (1978) age of 5200 cal yr B.P. for alluvial-fan deposits at North Creek, Jackson assigned a timing of 4000–4500 cal yr B.P. to P3.

Summary: In a review of paleoseismic data for Quaternary faults in Utah, the Utah Quaternary Fault Parameters Working Group (UQFPWG; Lund, 2005) reported a consensus chronology of surface-faulting earthquakes on the Nephi segment. The UQFPWG's consensus timing for the Nephi segment includes:

P1 <1000 (but possibly as recent as 400) cal yr B.P.
P2 ~3900 cal yr B.P.
P3 >3900 and <5300 cal yr B.P. for P3 (table 3).

However, Lund (2005) concluded that "the existing paleoseismic data for the [Nephi segment] are considered poorly

Table 2. *Numerical ages from the North Creek and Red Canyon trenches.*

Trench site, relation to earthquake[1]	Sample number[2]	Material sampled, dating method [3]	Lab reported ^{14}C or TL age[4]	Calendar correction applied to AMRT ages (yr)[5]	Calendar-corrected age range (cal yr B.P.)[6]	MRT-corrected age range (cal yr B.P.)[7]	Median age (cal yr B.P.)[8]
NC, min P1?	WC-12-80-10	Charcoal, AMS	0 ± 300	Calibrated	0–600	-	**300**
NC, min P1?	WC-12-80-4	Charcoal, AMS	250 ± 300	Calibrated	0–700	-	**400**
NC, max P1?	WC-12-80-2	Charcoal, AMS	300 ± 300	Calibrated	0–700	-	**400**
NC, max P1	WC-12-80-6	Charcoal, C	1110 ± 60	Calibrated	900–1200	-	**1100**
NC, max P1	WC-12-80-6	Charcoal, AMS	700 ± 250	Calibrated	300–1200	-	**800**
NC, max P1	WC-12-80-5	Charcoal, C	1350 ± 70	Calibrated	1100–1400	-	**1300**
NC, max P1	WC-12-80-5	Charcoal, AMS	1550 ± 300	Calibrated	900–2200	-	**1600**
NC, max P1	WC-12-80-8	Charcoal, AMS	1200 ± 300	Calibrated	600–1700	-	**1200**
RC, max P1	ITL-88	Bulk soil, TL	1300 ± 500	-	300–2300	-	**1300**
RC, max P1	ITL-67	Bulk soil, TL	1500 ± 400	-	700–2300	-	**1500**
RC, max P1	JRC-14	Bulk soil, C	2900 ± 90	+160	2900–3200	2400–3100	**2800**
NC, min P2	WC-12-80-7a	Bulk soil, C	3640 ± 75	+350	3800–4100	3300–4000	**3700**
NC, min P2	WC-12-80-7a	Bulk soil, AMS	1700 ± 300	0	1100–2300	600–2200	**1400**
NC, min P2	WC-12-80-7a	Bulk soil, AMS	3850 ± 400	+470	3500–5100	3000–5000	**4000**
NC, min P2	WC-12-80-7b	Bulk soil, C	1650 ± 50	0	1600–1800	1100–1700	**1400**
NC, min P2	WC-12-80-7c	Bulk soil, AMS	3894 +288/-278	+420	3800–4900	3300–4800	**4100**
NC, min P2	WC-12-80-7d	Bulk soil, AMS	1645 +270/-262	0	1100–2200	600–2100	**1400**
NC, min P2	WC-12-80-9	Charcoal, AMS	1389 +181/-177	Calibrated	900–1600	-	**1300**
RC, max P2	JRC-17	Bulk soil, C	1380 ± 120	0	1100–1600	600–1500	**1100**
RC, max P2	ITL-66	Bulk soil, TL	1700 ± 200	-	1300–2100	-	**1700**
RC, max P2	JRC-15	Bulk soil, C	3690 ± 170	+340	3700–4400	3200–4300	**3800**
RC, max P2	ITL-90	Bulk soil, TL	7000 ± 800	-	5400–8600	-	**7000**
NC, max P3?	WC-12-80-3	Bulk soil, C	2180 ± 80	0	2000–2300	1500–2200	**1900**
NC, max P3?	WC-12-80-3	Bulk soil, AMS	4500 ± 300	+650	4600–5800	4100–5700	**4900**
NC, max P3	USGSW-4057*	Charcoal, C	4580 ± 250	Calibrated	4600–5800	-	**5200**
NC, max P3	USGSW-4057*	Charcoal, AMS	4000 ± 400	Calibrated	3500–5500	-	**4500**
RC, min P3	JRC-16	Bulk soil, C	3550 ± 150	+300	3600–4200	3100–4100	**3600**
RC, max P3	ITL-48	Bulk soil, TL	14,600 ± 1200	-	12,200–17,000	-	**15,000**

[1] Trench sites: NC – North Creek (Hanson and others, 1981); ages summarized from Hanson and others (1982a, 1982b). RC – Red Canyon (Jackson, 1991). Relation of sample to earthquake timing: P1 – most recent paleoearthquake, P2 – second paleoearthquake, P3 – third paleoearthquake. Max and min indicate that samples represent maximum- or minimum-limiting time constraints per event.

[2] ITL indicates a thermoluminescence sample; all other samples were radiocarbon dated. *Sampled by Bucknam (1978), reported in Hanson and others (1981) as sample WC-12-80-11.

[3] C – ^{14}C conventional (gas proportional) methods, AMS – ^{14}C accelerator mass spectrometry, TL - thermoluminescence.

[4] Lab reported ^{14}C age (1 sigma).

[5] "Calibrated" indicates charcoal samples calendar calibrated using CALIB 5.0 radiocarbon calibration program (Stuiver and Reimer, 1993) and calibration dataset IntCal04 (Reimer and others, 2004). For bulk-soil samples, correction value is midpoint of 2-sigma, calendar-calibrated age minus mean ^{14}C laboratory age. No correction was applied if solar age deviated less than 150 years from the laboratory age. See text for expanded discussion.

[6] For charcoal samples, age range is >95% probability, calendar-calibrated, 2-sigma age distribution rounded to the nearest century. For bulk-soil ages, age range is ^{14}C laboratory age plus calendar correction plus/minus a doubled laboratory uncertainty. For TL ages, 2-sigma age range is TL laboratory age plus/minus a doubled laboratory uncertainty.

[7] MRT – mean residence time. For bulk soil samples, a 300-year correction was applied to bulk-soil 2-sigma age ranges by subtracting 500 years from the low end and 100 years from upper end of the range, following Nelson and others (2006).

[8] Median age is midpoint of 2-sigma age range (or MRT-corrected age range for bulk-soil samples) rounded to the nearest century.

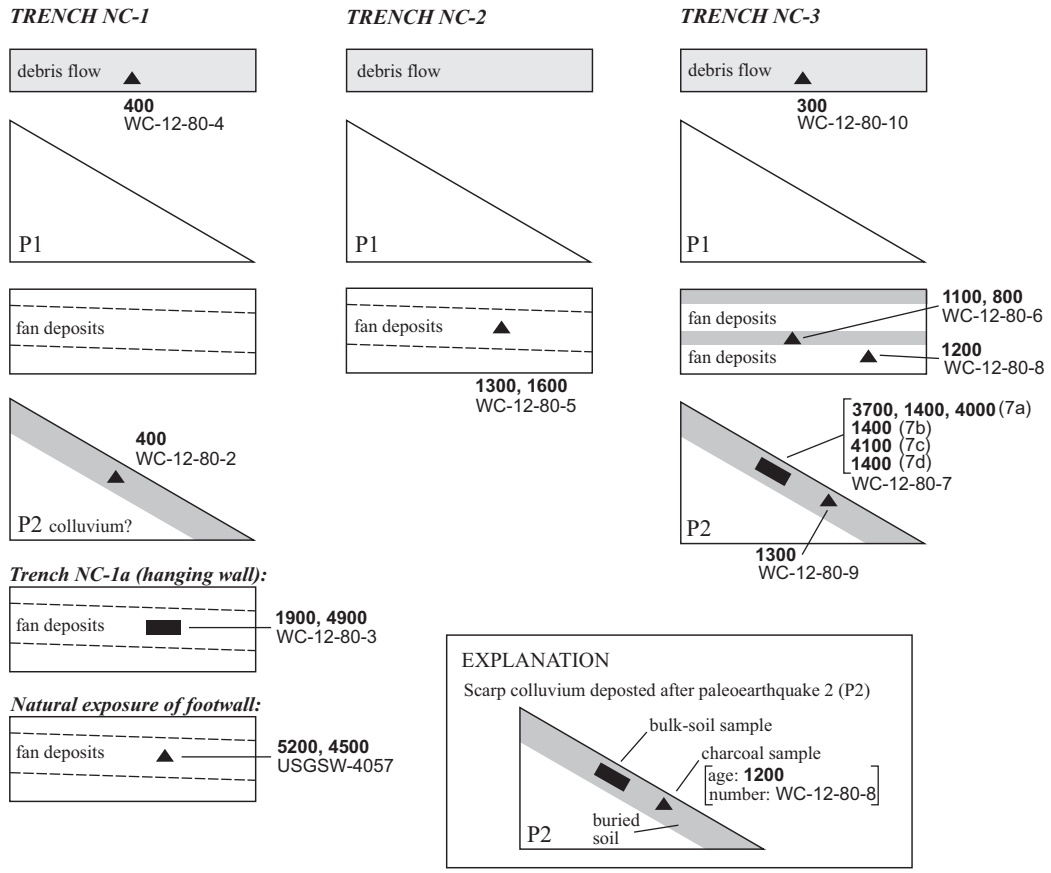

Figure 4. *North Creek trench site stratigraphy and sample locations, based on Hanson and others (1981, 1982a). Radiocarbon ages reported as calendar-calibrated mean ages of samples (in bold) corresponding with sample data given in table 2.*

Table 3*. Summary of paleoseismic earthquake-timing data for the Nephi segment.*

Earthquake	North Creek[1]	Red Canyon[2]	UQFPWG Consensus[3]
P1	>300–400 <800–1600	<1300–1500	<1000 ± 400, possibly as recent as 400 ± 100
P2	>1300–1400 >3700–4100	<1100–1700 <3800	~3900 ± 500
P3	<4500–5200*	>3600	>3900 ± 500 <5300 ± 700

Note: all ages in calendar years before present (1950). Age ranges represent possible minimum- (>) or maximum-limiting (<) time ranges based on published radiocarbon and TL ages for the Nephi segment (table 2). We excluded anomalous ages from North Creek sample WC-12-80-2 (400 cal yr B.P.) and Red Canyon samples JRC-14 (2800 cal yr B.P.), ITL-90 (7000 cal yr B.P.), and ITL-48 (15,000 cal yr B.P.), and also North Creek sample WC-12-80-3 (1900/4900 cal yr B.P.) due to uncertainty in the context of the sample.

[1] Based on Hanson and others (1981, 1982a, 1982b). *From Bucknam (1978).

[2] Based on Jackson (1991).

[3] Utah Quaternary Fault Parameters Working Group consensus earthquake timing from Lund (2005).

constrained, and multiple surface-faulting chronologies are possible depending on which ages are accepted and which are discarded."

One alternative paleoearthquake chronology includes P2 timing of between 1300 and 1700 cal yr B.P. This chronology disregards the older ages (between 3700 and 4100 cal yr B.P.) that constrain the event because the bulk-soil samples may have contained older organics from throughout or near the bases of the buried soils. At North Creek, five of seven ages constrain the minimum time of P2 to about 1300–1400 cal yr B.P., and at Red Canyon, two of four samples constrain P2 to a maximum of about 1100–1700 cal yr B.P. Additionally, we note that the Red Canyon samples with younger ages were collected from a relatively simple part of the trench exposure as opposed to samples dated at 3800 and 7000 cal yr B.P., which were collected from a relatively more complex part of the exposure, where an unrecognized graben structure adjacent to the main fault may have juxtaposed younger and older units (Jackson, 1991).

Scarp Morphology

Scarps along the Nephi segment produced by surface faulting show systematic changes in morphology with time, and thus provide a relative-age dating tool. DuRoss (2004) and DuRoss and Bruhn (2005) used fault-scarp mapping, profiling, and morphologic modeling (after Andrews and Bucknam [1987] and Mattson and Bruhn [2001]) to determine the vertical separation (i.e., fault displacement) and initiation time of scarps along both the northern and southern strands of the Nephi segment. The scarp-profile data indicate as much as 10 m of surface offset across Holocene alluvial-fan surfaces and 11–25 m of offset across older (approximately late Pleistocene) surfaces. DuRoss and Bruhn (2005) suggested an average of about 2 m of displacement per earthquake and a Holocene earthquake chronology including as many as five separate surface-faulting earthquakes having magnitudes of 6.5 to 7.1.

DuRoss and Bruhn (2005) used the scarp-profile data to formulate three separate fault-rupture scenarios and calculate fault slip rates and earthquake recurrence intervals. In their preferred scenario, DuRoss and Bruhn (2005) indicated three Holocene earthquakes on both the northern and southern strands, resulting in slip-rate estimates of 0.5 mm/yr and 0.7 mm/yr and recurrence intervals of 2100–4100 years and 2600–3300 years, respectively. Considering discrepancies in the paleoearthquake diffusion-based ages, amount of vertical displacement, and fault-scarp complexity and geometry along the segment, DuRoss and Bruhn (2005) suggested the possibility of both partial- and multi-segment ruptures on the two strands. They concluded that partial ruptures may be limited to the individual strands, and that multi-segment ruptures may involve the northern strand during Provo-segment earthquakes.

SANTAQUIN TRENCH SITE

Geologic Setting

The Santaquin trench site is about 1.6 km east of Santaquin, Utah, near the middle of the northern strand of the Nephi segment (figure 2). At the site, down-to-the-northwest surface faulting along the WFZ has displaced the apex of a Holocene alluvial fan that is incised into the Bonneville shoreline. We mapped the surficial geology at the site and in the surrounding area at about 1:10,000 scale (figure 5) using low-sun-angle aerial photographs, National Agricultural Imagery Program (NAIP, ca. 1975) and USGS digital aerial photographs (1993), and both hand-held and precision-grade GPS. Previous geologic mapping in the area includes 1:50,000-scale WFZ mapping by Machette (1992) and Harty and others (1997). We also used precision-grade GPS to generate a large-scale (0.5-m contour interval) topographic map of the site (figure 6) and to measure two long and four short profiles across fault scarps at the site (figure 5; plate 1), and two long profiles (GPS profiles 9 and 10; figure 5) across a faulted pre-Bonneville alluvial-fan surface south of the site. The detailed topographic map allowed us to study the morphology of the faulted Holocene alluvial-fan surface, and the fault-scarp profiles yielded scarp-height and net-surface-offset information. Additionally, the long GPS profiles, which extend tens of meters beyond the scarps, provide a record of the relative elevations of different alluvial-fan surfaces, and allowed us to compare them with shorter (31- to 66-m-long) profiles measured by DuRoss (2004) using a monopod-mounted laser rangefinder (plate 1).

The surficial geology at the Santaquin site includes a variety of late Pleistocene and Holocene deposits that record movement on the WFZ. Surficial deposits include hillslope and fault-scarp-derived colluvium, stream and debris-flow deposits related to alluvial-fan deposition, and deposits and geomorphic features (e.g., shorelines) related to late Pleistocene Lake Bonneville. At the site, surface-faulting earthquakes on the WFZ have displaced the majority of these deposits, forming moderate (<5 m high) to large (>10 m high) fault scarps and simple to complex fault patterns. The oldest surficial deposits at the site include pre-Bonneville alluvial-fan deposits (af4; figure 5), which are mostly limited to the footwall of the fault and uplifted about 40–60 meters above the youngest-fan deposits (figure 7). Latest Pleistocene lacustrine (Lake Bonneville) and Holocene alluvial-fan deposits have buried corresponding deposits on the downthrown side of the fault. However, southeast of the trench site, we mapped a remnant of af4 deposits on both the hanging-wall and footwall sides of the fault. Two long GPS profiles measured during this study (profiles 9 and 10, figure 5), and a shorter profile measured by DuRoss (2004), indicate scarp heights of 20–27 m and a net vertical offset across the fault zone of 16–22 m.

We mapped constructional wave-built platforms and deposits of sand and gravel (lbs and lbg; figure 5) related to the transgression and highstand shoreline of late Pleistocene Lake Bonneville. Lake Bonneville occupied the highstand shoreline between about 18,000 and 16,800 cal yr B.P. (D.R. Currey, University of Utah, written communication to UGS, 1996; see also Lund, 2005, table 4), when the lake level dropped catastrophically in response to erosion at the lake's outlet at Zenda, Idaho. The lake stabilized about 100 m lower at the Provo level, which is below the elevation of the trench site. On the footwall of the WFZ southeast of the trench site, the Bonneville shoreline is expressed as an eroded bedrock notch at an elevation of about 1560 m, and a boulder-strewn, wave-built platform between elevations of 1546 and 1560 m (lbg; figure 5). This part of the shoreline

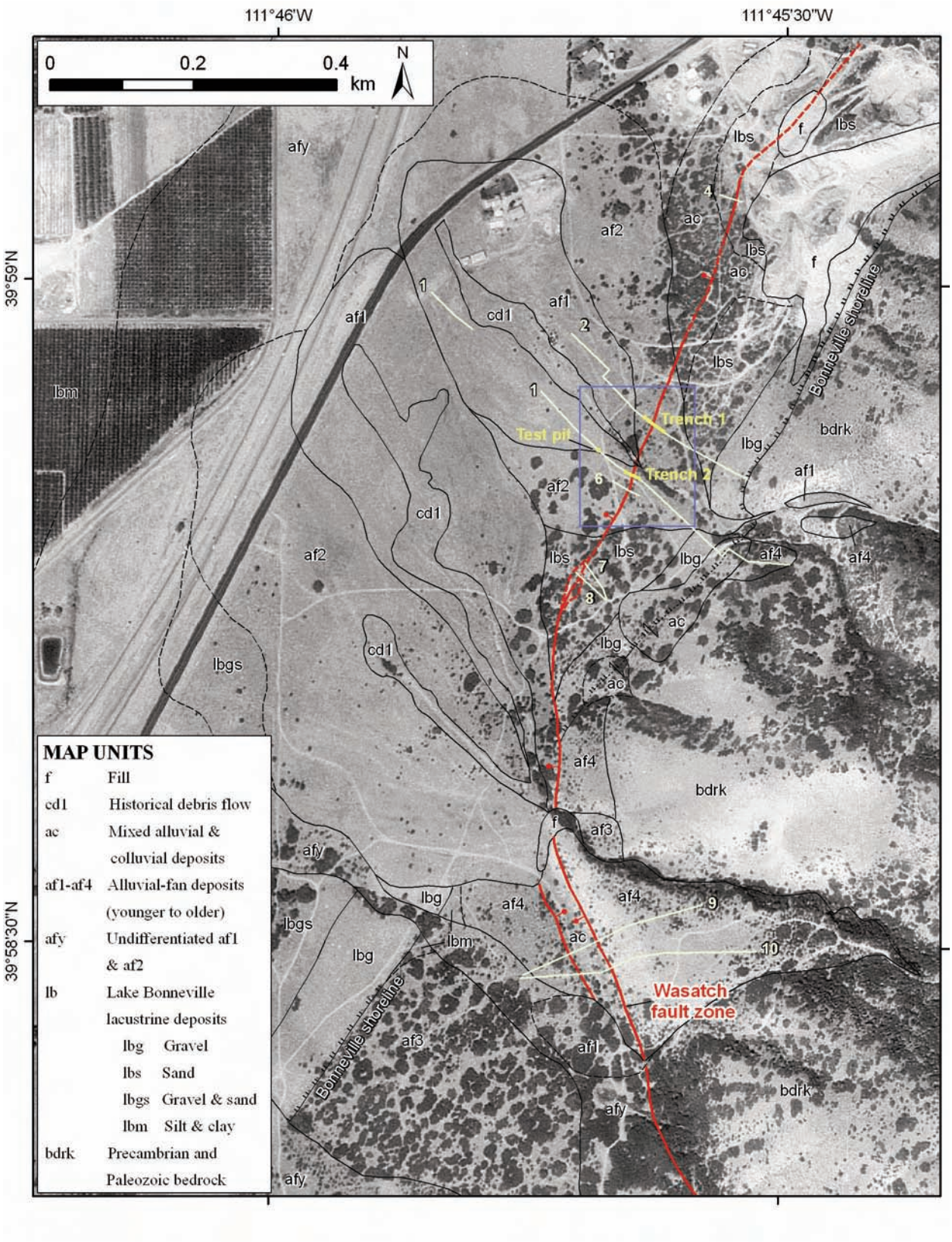

Figure 5. *Surficial geology of the Santaquin trench site and surrounding area. Yellow lines indicate fault trenches; green lines and numbers indicate GPS profiles. Red lines indicate trace of the Wasatch fault; ball and bar on downthrown site. Blue box is area of figure 6. Basemap is 1-m digital orthophoto.*

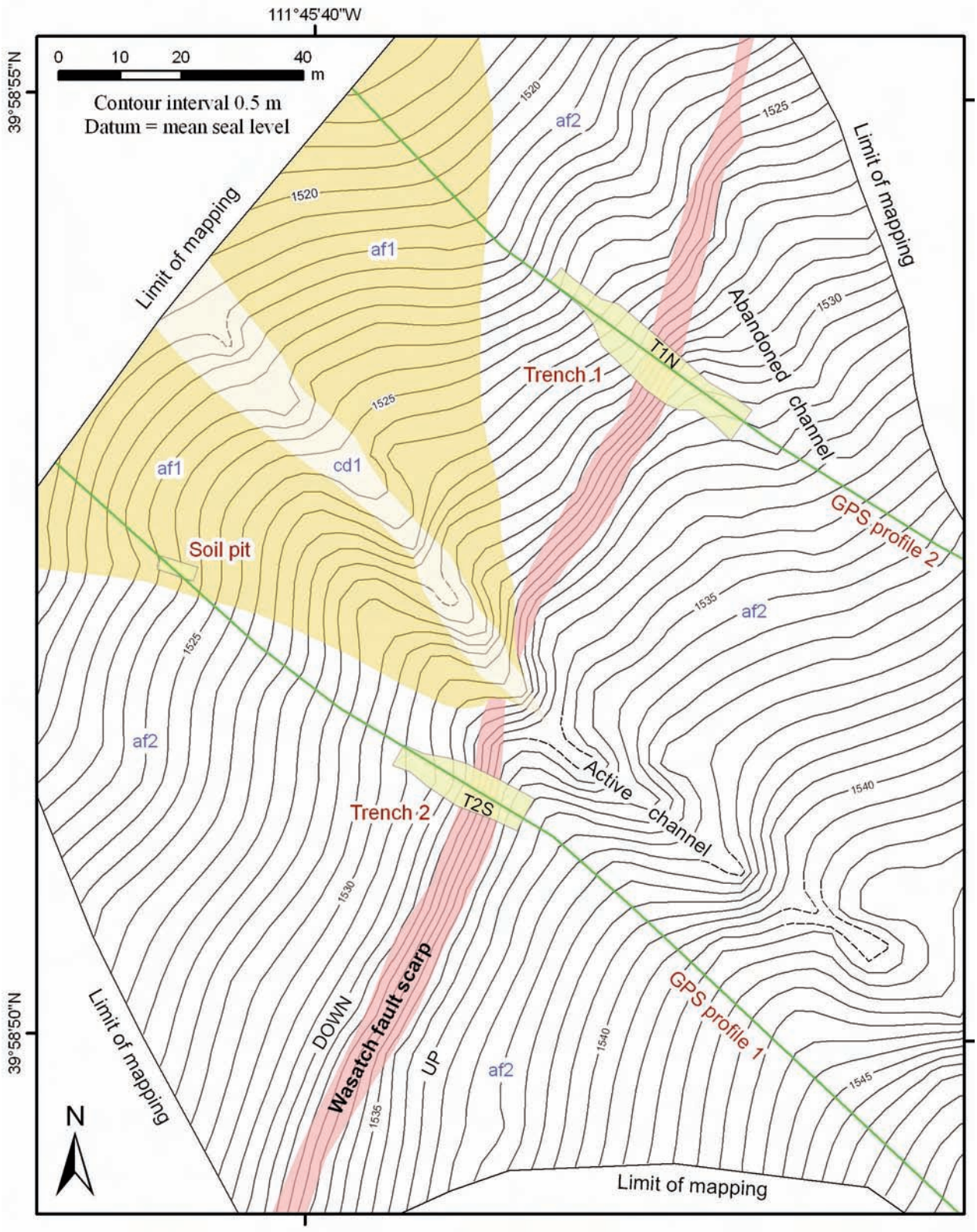

Figure 6. *Topographic map of the Santaquin trench site. Map generated from elevation data measured with precision-grade GPS. Red shaded areas denote the Wasatch fault scarp; "down" is downthrown side and "up" is upthrown side of the fault; yellow indicates excavated areas (T1N - trench 1 north wall, T2S - trench 2 south wall); green lines are GPS profiles (plate 1). See figure 5 for explanation of map unit symbols.*

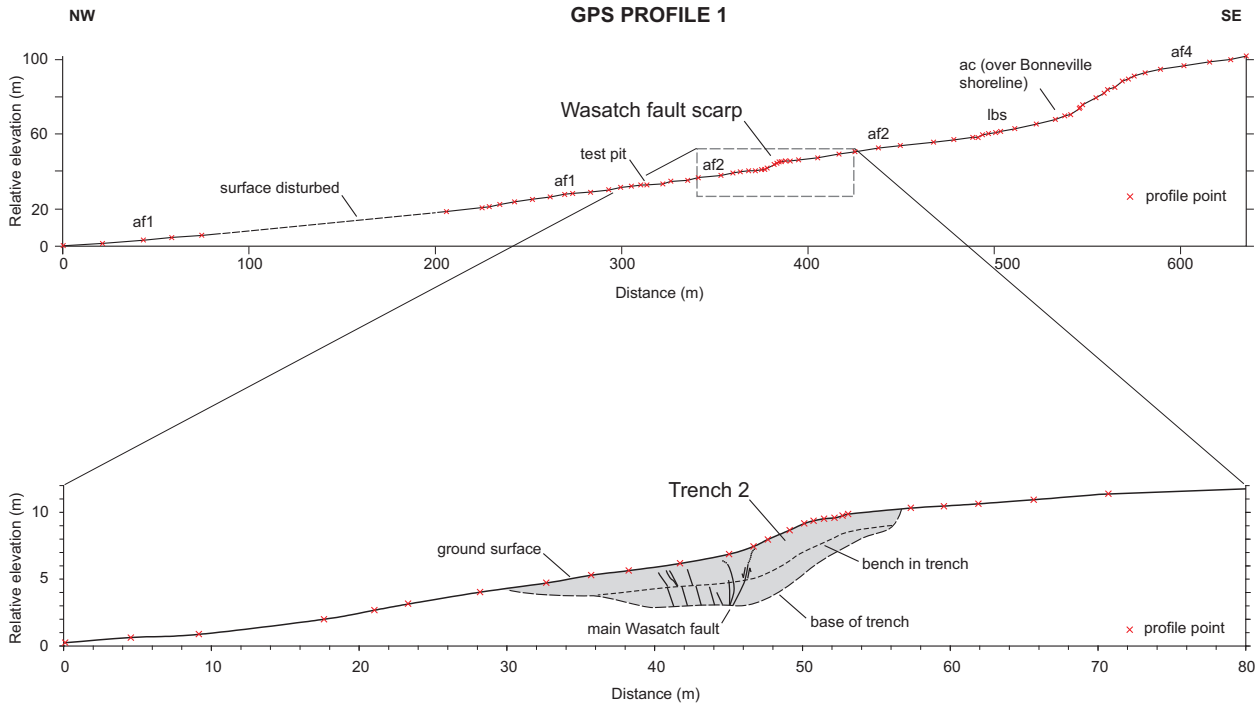

Figure 7. *GPS scarp-profile 1, measured across the Santaquin trench site, showing location of trench 2 and test-pit excavations. Geologic units and profile location are shown on plate 1.*

is coincident with the 5120-foot contour line on the U.S. Geological Survey Santaquin 7.5-minute topographic quadrangle. About 800 m southwest of the site, on the fault hanging wall, an equivalent shoreline is located slightly above the 5080-foot (1549 m) contour, which led M. Machette (USGS, verbal communication, 2004) and DuRoss (2004) to infer that the shoreline is displaced approximately 10 m across the fault. By re-evaluating and mapping the surficial geology at the site, including mapping the shorelines on aerial photographs draped over a 10-m digital elevation model for the area and comparing precision-grade GPS elevation data collected along the shoreline on both hanging-wall and footwall fault sides, we estimate 9 m of Bonneville shoreline elevation change across the WFZ.

We measured GPS profiles across 3.8- to 5.3-m-high scarps developed on Lake Bonneville nearshore sand deposits at the site (lbs; figure 5). GPS profile 4 (figure 5, plate 1) indicates about 3.4 m of vertical displacement, which we consider a minimum value because open-pit gravel mining has disturbed and completely removed parts of the ground surface a few meters above the crest of the scarp. GPS profiles 7 and 8 (figure 5) did not extend across the entire complex and diffuse fault zone, so we could not estimate vertical displacements. Despite these difficulties, the Bonneville shoreline displacement and scarp profiles indicate that at least two, and more likely three, earthquakes having 2–3 m of displacement per event have occurred after abandonment of the highstand shoreline at 16,800 cal yr B.P.

Following the retreat of Lake Bonneville, deposition at the site returned to an alluvial-fan environment, which initially was likely dominated by sediment reworked from the nearby Lake Bonneville sand and gravel deposits. Alluvial-fan deposition continued into the Holocene, with mixed stream and debris-flow deposits forming a well-defined alluvial-fan surface (af2; figure 5). During the Holocene, at least one surface-faulting earthquake on the Nephi segment ruptured across the site, uplifting the apex of the alluvial fan and forming a northeast-trending fault scarp (figure 6). The scarp, across which we excavated two trenches (figure 6), has a simple geometry, expressed as a single trace without an antithetic scarp evident at the surface. However, on the GPS profiles (e.g., figure 7) and on profiles collected by DuRoss (2004), a decrease in the slope of the alluvial-fan surface at the base of the scarp suggests that a narrow (less than 10-m-wide) graben formed along one or more down-to-the-east now-buried antithetic faults. GPS profiles 1, 2, and 6, and profiles P33, P34, P63, and P64 measured by DuRoss (2004) (plate 1) indicate that the scarp is 2.6–4.3 m high and has a surface offset (net displacement) ranging from 2.2 to 3.3 m (plate 1). Both scarp height and surface offset decrease to the north to about 2 m (based on profile P60 of DuRoss, 2004; plate 1). In this area, scarps are not well preserved, have been locally buried or modified by post-faulting alluvial-fan and colluvial deposits, are formed on noncohesive Lake Bonneville nearshore sand deposits (lbs; figure 5), and are obscured by gravel mining (figure 5).

Several kilometers north of the site (near Spring Lake; figure 2), Machette (1992) has mapped a single, approximately 4-m-high (3-m vertical offset) scarp on Holocene alluvial-fan deposits. North of this scarp, surface faulting continues for several kilometers before being concealed by Holocene alluvium near Payson (Machette, 1992). North of Payson, the northern end of the northern strand (figure 2) is marked by a 2-m-high scarp on the Benjamin fault (Machette, 1992), which is on Lake Bonneville silt and clay west of a faulted ridge of Tertiary tuffaceous sandstone (Solomon and others, 2006).

South of the Santaquin trench site, scarps having as much as 10 m of displacement are formed on Holocene to latest Pleistocene alluvial-fan surfaces along the western base of Dry Mountain, bordering Santaquin Canyon (Harty and others, 1997; DuRoss and Bruhn, 2005) (figure 2). These scarps continue for about 6 km south of the trench site and form the southern half of the northern strand, which is separated from the southern strand by a southwest-oriented cross fault in bedrock.

Following the most recent earthquake at the site, the locus of deposition on the alluvial-fan surface shifted to the northwest along the base of the scarp. The upthrown part of the fan surface became incised by stream flow, and alluvial sediment was transported farther from the apex of the fan before being deposited. This change in the area of active deposition on the fan is also evident in historical debris flows (e.g., cd1; figure 5), which have been deposited several hundred meters west of the range front. Using the large-scale (detailed) topographic map, we also identified an abandoned channel along the northeastern part of the alluvial fan (figure 6). This channel is displaced by the WFZ, but younger deposits limited to the hanging wall of the fault suggest intermittent activity following the surface-faulting earthquake, but prior to establishment and entrenchment of the modern channel to the southwest.

Trench Excavations

We excavated two bench-type trenches across a 3- to 4-m-high, northwest-facing fault scarp on a Holocene alluvial-fan surface (af2; figures 5 and 6). The trenches exposed (1) dominantly coarse-grained, gently northwest-dipping (slope parallel), bedded alluvial-fan sediments; (2) evidence for down-to-the-northwest fault displacement along main and subsidiary normal faults (figure 8); and (3) fault-scarp colluvium deposited after the most recent surface faulting. Trench 1 (north) was 36 m long and exposed 8 vertical meters (from base to top of trench) of alluvial-fan and colluvial deposits, which we subdivided into ten units. Trench 2 (south) was 22 m long and exposed about 7 vertical meters of alluvial-fan and colluvial deposits, which we subdivided into eight units. We also excavated a 1.7-m-deep test pit in organic-rich alluvial-fan sediments about 40 m downslope (northwest) of trench 2. The test pit exposed several stacked alluvial-fan deposits, which we subdivided into four units (plate 1).

We logged sedimentary and structural contacts at 1:20 scale (plate 1) on the north wall of trench 1, south wall of trench 2, and the test pit. We logged the north wall, rather than the south wall, of trench 1 as it exposed more distinct stratigraphic and structural relations. We used a total station to record the positions of nails and flagging used to mark the contacts, and projected the points to a single vertical plane (separately for each trench) parallel to the average orientation of the trench walls in the main fault zone. We then annotated and plotted the points for each trench for use as a template for detailed logging of stratigraphic and structural features (plate 1). We also logged the main fault zone in the trench 2 north wall at about 1:20 scale on a photomosaic of the exposure (plate 1), and show the important stratigraphic and structural relations exposed in the trench 1 south wall in figure 9. Stratigraphic unit descriptions are included in the appendix.

Radiocarbon Dating

We collected bulk samples of paleosols (buried soils) and detrital charcoal from both trenches and the test pit (table 4). The bulk-soil samples each consisted of several kilograms of organic material from the upper 5-10 cm of buried A horizons, or similar amounts collected from organic-rich debris flows. Detrital-charcoal samples were typically small, millimeter-sized pieces (table 4) that were incorporated into alluvial-fan sediments during transport and deposition. Since they are transported, they could be considerably older than the deposits containing them.

We sent 10 bulk-soil samples (STBS-1-3, 5, 7-12) to Paleo Research Institute (PRI) for the separation, recovery, and identification (plant genus and species) of organic material that would be suitable for radiocarbon analysis. Our preferred material consisted of charred, non-transported (i.e., non-detrital) macrofloral remains of a tree or shrub genus having a short age span (e.g., oak) and limited spatial occurrence. Radiocarbon dating of non-detrital charcoal of a particular plant or shrub genus is superior to obtaining apparent-mean-residence-time (AMRT) ages on bulk organics from buried soils (Puseman and Cummings, 2005), and represents a fundamental change in our recent Nephi-segment trench investigations from previous investigations. Previous investigations relied on the interpretation of AMRT ages, which is complex owing to the potential age range of organic material in the soil, and uncertainty in the inherited age (at the time of burial) of different organic fractions in the soil (Machette and others, 1992; Nelson and others, 2006).

We submitted eight charcoal fragments separated from bulk-soil samples (STBS-2, 3, 5, 7-9, 11, 12) and three detrital-charcoal samples (STRC-14, 16, 18) to Lawrence Livermore National Laboratory (LLNL) for AMS radiocarbon dating (table 4). Where possible, we submitted discrete charcoal fragments of a suitable plant genus separated from the bulk-soil samples. However, several bulk-soil samples yielded only small, disseminated charcoal fragments that PRI could not classify by plant genus (e.g., PRI recovered 36 hardwood charcoal fragments of an unidentified plant genus from sample STBS-2; table 4). For each of these samples, we aggregated multiple fragments for radiocarbon analysis because of the low mass (less than 0.001 g) of each individual charcoal fragment, resulting in a composite age for the charcoal separated from the bulk sample.

For samples consisting of multiple charcoal fragments collected from the matrix of debris flows (e.g., samples STBS-5, 7, 8, 11; table 4), we infer that a significant part of the composite age reflects an inherited but unknown age component from detrital charcoal. We are more confident in

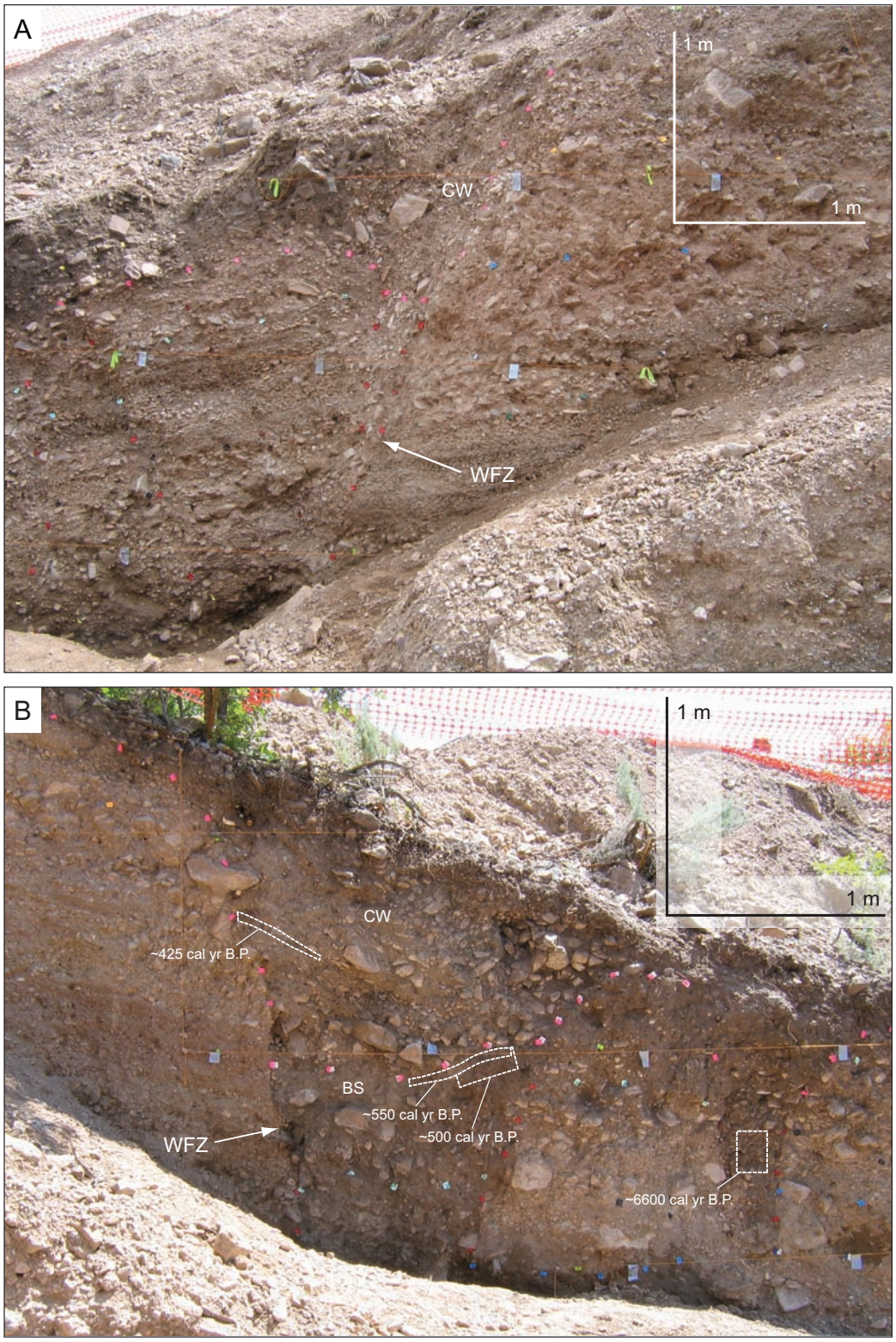

Figure 8. *Faulting exposed in the Santaquin trenches. (A) Trench 1 north-wall exposure of the Wasatch fault zone (WFZ) and colluvial wedge (CW). View to the northwest. (B) Trench 2 south-wall exposure of the WFZ, CW, and buried soil (BS). View to the southeast. Short-dashed lines indicate areas of bulk-soil samples; ages are midpoints of two-sigma, calendar-calibrated age ranges (table 5); see text for discussion. Note slightly different scales for the two photos.*

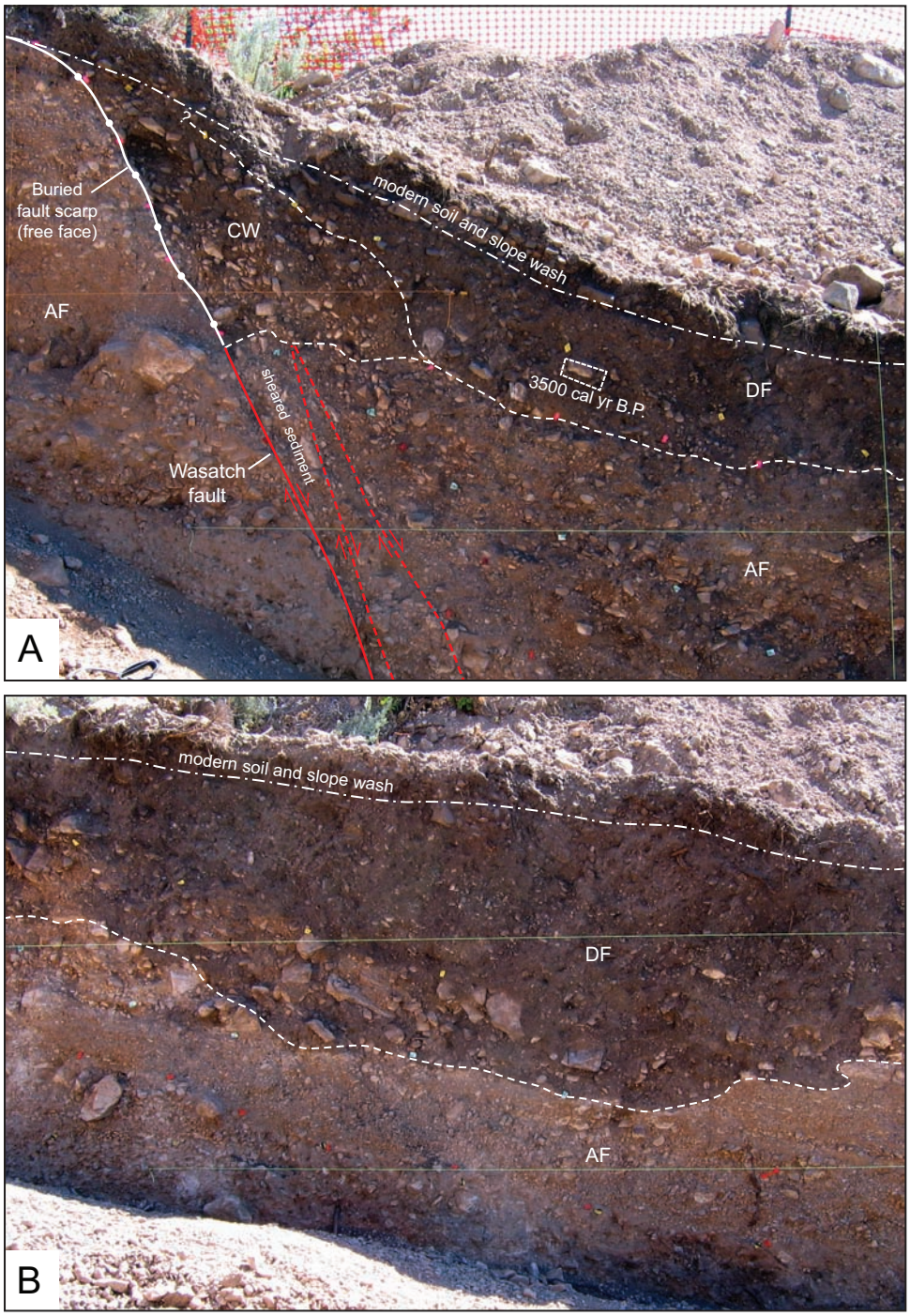

Figure 9. *Post-faulting debris flow (DF) exposed in trench 1 south wall, where it has (A) obscured the distal part of the MRE colluvial wedge (CW), and (B) buried older alluvial-fan deposits (AF) on the hanging wall of the WFZ. Horizontal level lines are 1 m apart. Centers of photos are approximately 5–6 m (horizontally) apart. View is to the southeast. The north wall of this trench is shown on plate 1.*

***Table 4**. Data for radiocarbon samples from the Santaquin trench site.*

Field No.[1]	Trench/Wall[2]	Sampled location relative to meter marks (m)[3]	Depth (m)[3]	Unit[4]	Unit notes[4]	Tectonic notes[5]	Sample notes[6]	Radiocarbon lab No.[7]	Lab-reported age (^{14}C yr B.P.)[8]	Calendar-calibrated, 2-sigma age range[9]	Median age of carbon (cal yr B.P.)[9]
STRC-1	T2/S/U	4, 5	0.9	5	D	FW, Max	(1) 2x2 mm	-	-	-	-
STRC-2	T2/S/U	13, 2	1.3	5	D	HW, Max	(2) 0.5x2 mm	-	-	-	-
STRC-3	T1/S/L	NA	3.2	-	D	HW, Max	(5) 1x2-3 mm	-	-	-	-
STRC-4	T1S/L	NA	3.5	-	D	FW, Max	(2) 0.5x1.5 mm	-	-	-	-
STRC-5	T1/N/L	28, 5.4	2.3	5	S	FW, Max	(1) 2x3 mm, (2) 2 1x2 mm	-	-	-	-
STRC-6	T1/S/U	NA	1.1	6	D	FW, Max	(1) 2x2 mm	-	-	-	-
STRC-7	T1/N/U	20.5, 4.7	0.9	5	D	FW, Max	(1) 1.5 x 1.5 mm (4) 0.5x0.5 mm	-	-	-	-
STRC-8	T1/N/U	11.7, 1.6	1.5	5	S	FW, Max	(1) 2x3 mm (1) 1.5x2 mm	-	-	-	-
STRC-9	T1/N/U	10.7, 1.3	1.7	5	BS, S	HW, Max	(1) 2x2 mm	-	-	-	-
STRC-10	T1/N/U	10.4, 1.1	1.8	5	D	HW, Max	(2) 2x2 mm	-	-	-	-
STRC-11	T1/N/U	6.0, 1.3	0.7	7	D	HW, Max	(2) 1x1 mm	-	-	-	-
STRC-13	T2/S/L	5.9, 2.9	2.5	1	S, H	FW, Max	(6) 1x1 mm	-	-	-	-
STRC-14	T2/S/L	5.4, 2.96	2.8	1	S, H	FW, Max	(1) 1x2 mm (4) 1x1 mm	120215	7830 ± 30	8540-8650	**8600**
STRC-15	T2/N/L	~3.3, -0.9	2.6	~3	H	FW, Max	(1) 2x3 mm (3) 1x1 mm	-	-	-	-
STRC-16	T1/N/U	5.9, 1.3	0.6	7	H	HW, Max	(1) 2x3 mm (1) 2x2 mm	120216	8345 ± 30	9290-9460	**9400**
STRC-17	T1/N/L	13.95, 0.4	3.1	3	D	HW, Max	(2) 1x3 mm	-	-	-	-
STRC-18	T1/N/L	13.9, 0.2	3.1	3	D	HW, Max	(5) 2x2 mm	120057	6055 ± 35	6800-7000	**6900**
STRC-19	T2/N/U	2.8, 0.9	3.2	-	D	HW, Max	(1) 2x2 mm	-	-	-	-
STBS-1[P]	T2/S/U	8.7, 2.7	1.5	7	BS, D	HW, Max*	10 x 20 cm; conifer species C, <0.001g	No date	-	-	-
STBS-2[P]	T2/S/U	9.4, 2.8	1.1	7	BS, D	HW, Max*	10 x 30 cm; (36) UH C, <0.001 g	120049	480 ± 35	450–550	**500**
STBS-3[P]	T2/N/U	3.2, 0.9	0.8	-	BS, D	HW, Max	10 x 22 cm; (5) oak (*Quercus*) C, 0.003 g	120050	1590 ± 30	1410–1540	**1500**
STBS-4	T2/N/U	6.3, 2.1	1.0	-	BS, D	HW, Max	10 x 40 cm; burrow nearby	-	-	-	-
STBS-5[P]	T1/N/U	14.7, 3.3	0.3	8	BS, D	HW, Max	10 x 25 cm; (8) UH C, 0.002 g	120051	2280 ± 35	2160–2250/2300–2350	**2200**/**2300**
STBS-6	Test pit	3, 1.3	0.4	3	D	HW, Min	12 x 18 cm	-	-	-	-
STBS-7[P]	Test pit	2.2, 0.8	0.9	2a	D	HW, Min	12 x 40 cm; (28) UH C, 0.004 g	120052	3455 ± 40	3630–3840	**3700**
STBS-8[P]	T1/S/U	NA	0.5	-	BS, D	HW, Max	12 x 23 cm; (52) UH C, 0.003 g	120053	3300 ± 35	3450–3620	**3500**
STBS-9[P]	T2/S/U	8.4, 3.5	0.75–0.8	8b	OS, C	HW, Min*	7 x 27 cm; (7) UH C, 0.002 g	121667	400 ± 45	300–550	**425**
STBS-10[P]	T2/S/U	9.2, 3.8	0.1	8c	MS, C	HW, Min	10 x 25 cm; no charcoal	-	-	-	-
STBS-11[P]	T2/S/U	10.6, 2.65	0.8	8a	FF	HW, Max	15 x 28 cm; (1) oak (*Quercus*), (7) UH C, <0.001g	121668	5770 ± 60	6410–6720	**6600**
STBS-12[P]	T2/S/U	9.1, 2.7	1.2	7	BS, D	HW, Max*	5 x 40 cm; (1) oak (*Quercus*), (40) UH C, 0.004 g	121666	525 ± 35	500–600	**550**
STBS-13	T2/S/U	9.3, 2.8	1.1	7	BS, D	HW, Max	5 x 40 cm	-	-	-	-
STBS-14,15	T1/S/U	NA	0.8–0.9	-	C	HW, Min	(2) 20 x 15–20 cm	-	-	-	-

[1]STRC denotes charcoal samples; STBS denotes bulk-soil samples. Sample STRC-12, a gastropod shell fragment, is not included in the table. [P]Bulk-soil samples submitted to Paleo Research Institute.
[2]T1 – Trench 1, T2 – Trench 2, N – north wall, S – south wall, U – upper wall (above bench), L – lower wall (below bench).
[3]Location (horizontal, vertical) on reference (level) lines used to map trench walls, NA – not applicable (wall photo-logged). "Depth" is depth below ground surface.
[4]Unit numbers on trench logs (appendix); FF – fissure fill, D – debris flow, S – stream, H – hyperconcentrated flow, C – colluvium, BS – buried soil, OS – organic stringers, MS – modern soil.
[5]FW – footwall, HW – hanging wall, Max – sample age constrains maximum time since earthquake, Min – sample age constrains minimum time since earthquake (* indicates a close minimum or maximum time constraint).
[6]Number (in parentheses) and size of charcoal fragment(s) or bulk-soil excavation area. For samples STBS-1-3, 5, 7-12, the type and weight of organic material identified by Paleo Research Institute (Puseman, 2005) is noted; UH – Unidentified hardwood, C – charcoal.
[7]All samples processed at Lawrence Livermore National Laboratory Center for Accelerator Mass Spectrometry.
[8]Lab-reported age is ± one sigma; delta^{13}C value is -25, Libby half-life used is 5568 years.
[9]Calendar calibrated using CALIB 5.0 (Stuiver and Reimer, 1993) and calibration dataset IntCal04 (Reimer and others, 2004). Median age represents midpoint of two-sigma age range, rounded to the nearest quarter (STBS-9), half (STBS-12), or full century.

ages based on multiple charcoal fragments separated from buried soils (e.g., samples STBS-2, 3, 9, 12; table 4). Although we cannot discount the possibility of detrital-charcoal fragments in these samples, the large number of dated charcoal fragments (likely burned in place) serves to minimize the effect of an inherited age component. Additionally, we consider these composite ages superior to AMRT ages as they represent an average age for disseminated charcoal collected from the uppermost (likely youngest) parts of buried soil horizons, rather than an average age for all of the organics incorporated into the soil over its entire period of development.

We report radiocarbon ages in calendar years before present (A.D. 1950) (cal yr B.P.), calibrated using the CALIB 5.0 radiocarbon calibration program (Stuiver and Reimer, 1993) and the non-marine calibration dataset IntCal04 (Reimer and others, 2004). We did not apply a laboratory uncertainty multiplier or sample age span, the latter of which uses a moving average based on the average life span of carbon in the sample, which we consider unknown. Calendar ages cited in the text represent the midpoint of the calendar-calibrated, two-sigma age range, rounded to the nearest century (table 4) to account for uncertainties in the continuity and timing resolution of stratigraphy bracketing the surface-faulting event, and the stratigraphic and structural context of the sample (Seitz, 1999). These sources of earthquake-dating uncertainty commonly far outweigh laboratory or analytical uncertainties (Seitz, 1999; Nelson and others, 2006).

SANTAQUIN PALEOSEISMIC INVESTIGATION

Stratigraphy

Pre-Faulting Alluvial-Fan Deposits

The majority of alluvial-fan deposits exposed at the Santaquin trench site pre-date the timing of the most recent surface-faulting earthquake (MRE). The deposits primarily consist of stream and debris-flow deposits, including high-energy sheet-flood and channel deposits (e.g., unit 1 in the trench 1 north wall [T1N] and trench 2 south wall [T2S]; plate 1); poorly sorted, massively bedded, and mostly matrix-supported debris-flow deposits (e.g., T1N unit 3 and T2S unit 5; plate 1); and mixed stream and debris-flow deposits (hyperconcentrated flows of Giraud, 2005; e.g., T1N unit 2 and T2S unit 3; plate 1). Most alluvial-fan units maintain a consistent thickness across the fault zone (e.g., T2S unit 5; plate 1), suggesting there was no preexisting scarp at the time of deposition. We also mapped units exposed on only the hanging wall or footwall of the fault (e.g., T1N unit 6; plate 1).

Alluvial-fan deposits in both trenches range in age from early to mid-Holocene. The oldest deposits (unit 1 in T1N and T2S; plate 1) comprise stacked, well-sorted, and thinly bedded sand and gravel lenses, which we interpret as reworked from Lake Bonneville shoreline beach deposits and wave-built terraces located above the site. Additionally, detrital charcoal from unit 1 (T2S unit 1) near the base of the trench in the fault footwall yielded an age of 8600 cal yr B.P. (7830 ± 30 ^{14}C yr B.P.; STRC-14, table 4), although this age may include an unknown inherited component. Between unit 1 and scarp-derived colluvium in trench 1, we mapped a vertical sequence of thin-bedded sand- and pea-gravel-rich stream deposits interbedded with debris-flow deposits (T1N units 2-7; meter marks 17 horizontal, 0-4 vertical; plate 1) that are mostly continuous in both the hanging-wall and footwall exposures. Detrital charcoal from T1N unit 3 yielded an age of 6900 cal yr B.P. (6055 ± 35 ^{14}C yr B.P.; STRC-18, table 4), which we consider to be the best estimate for the age of the oldest pre-faulting units exposed in the fault hanging wall of T1N (plate 1). The youngest pre-faulting unit in trench 1 is a hyperconcentrated-flow deposit (T1N unit 7; plate 1); detrital charcoal collected from this deposit 0.6 m below the ground surface (T1N meter marks 5.9, 1.3; plate 1) yielded an age of 9400 cal yr B.P. (8345 ± 30 ^{14}C yr B.P.; STRC-16, table 4). However, since this age is significantly older than the estimate for the underlying unit 3 (6900 cal yr B.P.), we believe the higher, older charcoal had a significant inherited age when entrained in T1N unit 7. In trench 2, several stacked, hyperconcentrated- and debris-flow deposits (T2S units 2-7; plate 1) overlie unit 1 and underlie scarp-derived colluvium unit 8 (figures 8b and 9; plate 1); however, no numerical age control was obtained for these deposits.

Alluvial-fan deposits exposed in the Santaquin trenches show evidence for a single surface-faulting earthquake. Soils developed on the alluvial-fan deposits, faulted down, and subsequently buried by scarp-derived colluvium provide the best evidence and chronological control for the surface-faulting earthquake. In trench 2, several unidentified charcoal fragments isolated from a buried soil formed on unit 7 (T2S meter marks 9, 2.8; plate 1) yielded an age of 500 cal yr B.P. (480 ± 35 ^{14}C yr B.P.; STBS-2, table 4). We collected the upper 5 cm of the buried soil from a similar location (table 4); charcoal from one oak and several unidentified plants yielded an age of 550 cal yr B.P. (525 ± 35 ^{14}C yr B.P.; STBS-12, table 4), which is a maximum for soil burial. In the north wall of trench 2, we mapped similar alluvial-fan deposits below scarp colluvium. The youngest pre-faulting unit includes two stacked debris-flow deposits (T2N units 2a and 2b; plate 1) below scarp colluvium (T2N unit 3; plate 1). We mapped a weak buried soil on unit 2a, which underlies unit 2b; charred oak (*Quercus*) fragments from the soil yielded an age of 1500 cal yr B.P. (1590 ± 30 ^{14}C yr B.P.; STBS-3, table 4). We were unable to find material for radiocarbon dating from unit 2b, which directly underlies scarp-colluvial unit 3 (plate 1). In the eastern part of the fault zone, unit 2b either pinches out or becomes indistinguishable from unit 2a. In this part of the exposure, scarp colluvium overlies a buried soil on undifferentiated unit 2 (plate 1); however, we were unable to date the soil in this location because of extensive burrowing and bioturbation. In trench 1, alluvial-fan unit 7 is overlain by scarp-derived colluvium (T1N unit 8a and 8b, meter marks 17.1, 3.9; plate 1) in the fault zone; however, no soil is present on the faulted fan deposits. We suspect that a weak soil formed on unit 7, as evidenced by numerous burrows near the top of the unit (e.g., near T1N meter marks 17, 3.8; plate 1), but was modified or obscured during deposition of a post-faulting debris flow (T1N unit 9; plate 1).

Fault-Scarp Colluvium

Fault-scarp-derived colluvium exposed at the Santaquin trench site post-dates the MRE. The colluvium consists of

wedge-shaped deposits (tectonic colluvial wedges) of loose, moderately well-sorted, and thinly bedded silt, sand, and gravel mixed with soil-organic matter (unit 8 in T1N and T2S; plate 1). In both trenches, scarp colluvium is exposed on the down-thrown sides of the fault, partially burying the faulted alluvial-fan surface and soil adjacent to the scarp free face (figure 8; plate 1). These scarp-derived colluvial wedges are the characteristic stratigraphic signature of a normal-slip, surface-faulting earthquake (e.g., Schwartz and Coppersmith, 1984; McCalpin, 1996).

Even though the scarps are rather large, we only exposed a single scarp-derived colluvial deposit in both the north and south walls of trench 1 (figures 8a and 9a; plate 1). In both exposures, colluvium has buried part of the scarp free face and is at least 80 cm thick, but stratigraphic and structural relations suggest that the toe of the colluvial wedge has been modified or obscured by an organic-rich, post-faulting debris flow (T1N unit 9, meter marks 17, 4; plate 1). Because of possible post-faulting erosion, as well as disturbance of the upper part of the wedge during trench excavation, we could not estimate the area of the colluvial wedge exposed in trench 1. Material below the scarp colluvium in the area of the main fault zone consists of well-sorted, thin-bedded stream deposits (e.g., T1N unit 5; plate 1) and matrix-supported debris-flow deposits (T1N units 3 and 4; plate 1) that are exposed in both trench walls and are continuous for tens of meters on both sides of the fault zone.

The south wall of trench 2 exposed good evidence for a single scarp-derived colluvial deposit. The colluvium has buried part of the scarp free face, filled a 1.6-m-wide fault-bounded graben, and buried a well-developed A horizon formed on T2S unit 7 (figure 8b; plate 1). The exposure of scarp colluvium tapers to the northwest from the base of the scarp (plate 1) and has a maximum height of about 1.5 m, a width of 3.6 m, and an area of 2.7–3.2 m^2. This area of colluvium is similar to the potential area of material eroded from the footwall of 2.8–4.2 m^2, determined by projecting the top of T2S unit 7 to a projection of the main trace of the Wasatch fault. The similar areas suggest that a closed system between scarp erosion and colluvial-wedge deposition developed after a single surface-faulting earthquake at the site. Based on the geometry and texture of the colluvial wedge (including strong slope-parallel fabric), we infer that the coarse lower part of the colluvium and a 50-cm-wide area of accumulated cobbles (T2S meter marks 9.5, 3.5; plate 1) represent the early colluvial-wedge debris facies (T2S unit 8b). We mapped the more organic-rich, finer grained, upper part of the wedge (e.g., T2S meter marks 9, 3.8; plate 1) as the later colluvial-wedge wash facies (T2S unit 8c) (following nomenclature of Nelson, 1992).

We submitted an aggregate of seven charcoal fragments of an unidentified plant genus from within the T2S colluvial wedge. The fragments are derived from a bulk-soil sample collected from a 2- to 4-cm-thick by 1.1-m long, weakly developed, scarp-slope-parallel stringer of soil organics (meter marks 8.3, 3.5; plate 1) present in the lower half of the colluvial wedge. The resulting age of 425 cal yr B.P. (400 ± 45 ^{14}C yr B.P.; STBS-9, table 4) suggests that the organic stringer is either (1) a weak soil developed on the surface of the colluvial wedge during a hiatus in colluvium deposition, or (2) soil-organic matter reworked from the modern (post-MRE) alluvial-fan soil on the fault footwall during an early phase of colluvial-wedge deposition. We prefer the latter interpretation because (1) several weak organic stringers are present, rather than a single thicker soil horizon, (2) the stringers are laterally discontinuous and taper toward the toe (distal part) of the wedge, and (3) the bases of the stringers are abrupt and regular, suggesting that the organic matter was transported to the colluvial wedge. However, in either case, the young age and stratigraphic position of the organic stringer, and lack of modern burrows (which could introduce younger material from the surface), indicate that the stringer formed after the MRE and initial burial of the faulted alluvial-fan surface at 500–550 cal yr B.P. (480–525 ^{14}C yr B.P. based on samples STBS-2 and STBS-12, table 4).

Scarp-colluvial deposits exposed in the north and south walls of trench 2 are somewhat different owing to the fault zone geometry. Scarp colluvium in the trench 2 north wall consists of two separate (eastern and western) colluvial-wedge deposits (plate 1), with a combined area of 2.5–3.0 m^2, as compared to the 2.7–3.2 m^2 south-wall colluvial exposure. The eastern colluvial wedge principally consists of mixed sand and gravel that unconformably overlies a faulted, fractured, and burrowed paleosol. The colluvium fines upward and toward the buried free face, and eventually merges with overlying modern soil and slope wash. We interpreted the lower, coarse part of the deposit, which contains slope-parallel clasts and organic-rich lenses, as the colluvial-wedge debris facies, and the upper, fine-grained part, which likely formed due to slope-wash processes, as the colluvial-wedge wash facies. The western colluvial wedge is about half as thick as the eastern wedge; consists of loose, poorly sorted silt, sand, and pea-sized gravel (similar to the wash facies of the eastern wedge); and overlies a 0.3- 0.5-m-thick debris flow (T2N unit 2b, plate 1). The debris flow tapers to the southeast and was not identified below the eastern wedge. The combined maximum thickness of both wedges in the trench 2 north wall is approximately 1.5 m.

Fissure-Fill Deposit

We mapped a fissure-fill deposit (unit 8a) in the trench 2 south wall that post-dates the MRE. The fissure fill includes a mixture of alluvial-fan deposits and soil-organic matter overlain by scarp-derived colluvium (T2S meter marks 10.6, 2.5; plate 1). Pre-MRE stratigraphic units and two buried soils, one radiocarbon dated at 1500 years and formed among alluvial-fan deposits in the north wall (plate 1) and the other dated at 500–550 years (STBS-2 and -12; table 4) and developed on the youngest alluvial-fan deposits in the south wall (plate 1), are displaced across the fissure. Charcoal fragments of an unidentified plant genus separated from a bulk-soil sample from the lower part of the fissure yielded an unexpectedly old age of 6600 cal yr B.P. (5770 ± 60 ^{14}C yr B.P.). This date is probably from detrital charcoal deposited in the fissure but reworked from the adjacent alluvial-fan deposits. This scenario could result in a radiocarbon age significantly older than the time of fissure formation, similar to the 9400 cal yr B.P. age for sample STRC-6 collected from one of the youngest faulted deposits in trench 1 (T1N unit 7; plate 1).

Despite the old radiocarbon age from unit 8a (fissure fill), we interpret the fissure as having formed during the MRE at the site. Evidence for a young fissure is exposed in

the south trench wall, where the fissure extends to within 30–40 cm of the ground surface, is stratigraphically younger than the buried soil dated at 500–550 years, is directly overlain by scarp-derived colluvial-wedge units 8b and 8c, and is formed along a main antithetic fault related to the MRE (plate 1). In the north wall, the same antithetic fault displaces all of the pre-MRE alluvial-fan deposits, which contain a buried soil dated at 1500 years. We have more confidence in the ages of the buried soils (500–550 and 1500 cal yr B.P.) than in the age of the fissure-fill material (6600 cal yr B.P.) because the fine-grained soils are less likely to include old detrital material transported to the site. Attributing the fissure to the MRE is also in agreement with the trench 1 exposure, where we mapped distinct colluvial-wedge deposits associated with the MRE above laterally continuous stream and debris-flow deposits (T1N units 2-7; plate 1) and found no evidence for an earlier earthquake.

We found no stratigraphic evidence that the fissure is related to an earlier earthquake. The fissure could have formed during a possible earlier (second) earthquake (P2) at the site following deposition of T2S unit 7 (plate 1) and then been faulted along the antithetic fault during the MRE. However, we consider this possibility unlikely because the MRE colluvium is in sharp stratigraphic contact with the soil on unit 7 (T2S meter marks 10, 3.3; plate 1), and no P2-related colluvium or evidence for its removal by alluvial-fan processes is present below the MRE colluvium. Additionally, we found no substantial indirect evidence, such as fault terminations and differential displacement, for a penultimate event at the site. Alternatively, we could have misinterpreted the origin of T2S unit 7 in the fault zone, but if mapped as older scarp colluvium, the deposit would have to be limited to the 1.6-m-wide graben adjacent to the main fault. In the fault zone, unit 7 is stratigraphically below the T2S colluvial wedge (unit 8) and consists of randomly oriented cobbles suspended in an organic, fine-grained matrix (e.g., T2S meter marks 8.8, 2.6; plate 1) characteristic of a debris-flow deposit. On the fault hanging wall, unit 7 continues to the northwest away from the fault zone for more than 11 m where it is in conformable stratigraphic contact with T2S unit 6. In the north-wall exposure (plate 1), we did not identify any scarp-derived colluvial material above units 2 and 3 (below the MRE colluvium; plate 1), which were continuous along the hanging wall and included numerous randomly oriented cobbles suspended in organic-rich matrix, which is typical of debris-flow deposits in this trench.

Post-Faulting Alluvial-Fan Deposits

In trench 1, we mapped a post-faulting alluvial-fan deposit (T1N unit 9; plate 1) that possibly modified or obscured the distal part of the scarp-derived colluvial wedge. In both north- and south-wall exposures of the hanging wall, we mapped a cobble-rich debris-flow deposit that has partially buried scarp colluvium, and in the south-wall, filled a channel incised several tens of centimeters into older, faulted alluvial-fan deposits (figure 9b). The debris-flow deposit has a very organic-rich matrix and increases in thickness from about 5 to 30 cm where exposed in the north wall of the trench (e.g., T1N meter marks 6-8, 1.7; plate 1) and reaches a maximum of about 1.5 m thick in the south wall (figure 9b). This correlation between the north- and south-wall exposures is based on similarities in the color and texture of the deposits (dark yellowish brown, silty gravel with organic fines and cobbles; appendix) and the abrupt base of the deposit, which overlies and has filled a channel formed in older stream deposits (e.g., T1N meter marks 15.2, 3.1; plate 1).

The surface morphology near trench 1 suggests that younger (post-MRE) alluvial-fan deposits are more extensive on the downthrown side of the fault. The deposits form a small, about 30-m-wide alluvial fan, which is sourced from a now-abandoned channel within the older (pre-faulting) alluvial-fan deposits on the upthrown side of the fault just north of trench 1 (figure 6) and has partly buried the fault scarp. Detrital charcoal fragments from the base of the debris flow in the north trench wall yielded an age of 2300 cal yr B.P. (2280 ± 35 ^{14}C yr B.P.; STBS-5, table 4). Numerous detrital-charcoal fragments from a bulk sample collected from the base of the debris flow in the south wall (figure 9a) yielded an age of about 3500 cal yr B.P. (3300 ± 35 ^{14}C yr B.P.; STBS-8, table 4). The antiquity and 1200-year difference of these ages for known post-MRE deposits suggest that most of the dated charcoal fragments had an inherited age at the time of incorporation into the debris flow. This is consistent with the anomalously old 9400 cal yr B.P. sample from T1N unit 7.

Test Pit

We excavated the test pit on the hanging wall of the Wasatch fault (west of trench 2) to investigate the contact between pre- and post-faulting alluvial-fan deposits (af2 and af1, respectively; figure 5). We exposed four stacked, gently northwest-dipping debris flows, which are poorly sorted (bimodally distributed) and contain brown, organic-rich matrix and randomly oriented gravel and cobble clasts (plate 1). The middle two units (2 and 3; plate 1) consist of 0.3- to 0.4-m-thick upward-coarsening debris flows. We found no evidence for fault deformation in the deposits, and based on alluvial-fan geomorphology, we suspect that the uppermost deposits in the test pit are post-faulting. A lack of well-developed buried soil in the exposure makes this determination equivocal, thus we are uncertain as to the age of these units relative to surface faulting at the site. We collected bulk organics from the top of a lower flow (bulk sample STBS-7 from unit 2), which yielded numerous charcoal fragments radiocarbon dated at 3700 cal yr B.P. (3455 ± 40 ^{14}C yr B.P.; table 4). The radiocarbon age suggests that the debris flow was deposited prior to the MRE; however, the age may have an inherited component, as the charcoal fragments sampled and dated are likely detrital.

Structure

Trench 1

Trench 1 exposed a narrow, down-to-the-northwest normal-fault zone (plate 1). In the north wall (figure 8a) the zone is 1.2–2.4 m wide (T1N horizontal meter marks 15.1–17.7; plate 1) and consists of a main, normal-fault shear zone (F1; T1N meter marks 17.1, 0; plate 1) as much as 30 cm wide with well-developed shear fabric (clast long axes parallel to plane of fault), an antithetic reverse fault (F2; T1N

meter marks 16.6, -0.8; plate 1), and an antithetic normal fault (F3; T1N meter marks 16.2, -0.5; plate 1). The azimuth and dip (using the right-hand rule) of the main fault (F1) are about 200°/74° NW to 215°/65° NW, but dips as steep as 84° NW were found near the base of the exposure; the subsidiary faults dip 65°–86° SE. We mapped a minor, discontinuous fracture subparallel to the subsidiary faults within the fault zone and a continuous 62°–70° northwest-dipping fracture about 5–6 m southeast of the fault zone (T1N horizontal meter marks 22-24.5; plate 1). Faults and fractures in the trench terminate upward at the contact between T1N units 7 and 9.

The vertical displacement of contacts between units that cross the entire fault zone in trench 1 ranges from 2.8 to 3.1 m (average of 3.0 m; table 5). This is similar to the net vertical surface offset of 3.3 m determined from our long GPS scarp profile (GPS profile 2; figure 5; plate 1). Shorter scarp profiles (P63 and P64; plate 1) measured by DuRoss (2004) indicate less surface offset (2.2–2.5 m), but these values are likely minima since the profiles were restricted to the surface of the ~1-m-thick, post-faulting debris flow (T1N unit 9; plate 1) on the hanging wall. Vertical-displacement estimates across the subsidiary faults are smaller (10–30 cm) and complex, including faults that change in orientation and sense of displacement from the north to south trench wall. We interpret this complexity to represent differential movement of large, intact blocks of strata that were down-dropped adjacent to the main fault. A graben did not form on the hanging wall due to a lack of significant antithetic displacement across the blocks.

Trench 2

Trench 2 exposed a 5-m-wide normal-fault shear zone (plate 1). In the south wall, the zone includes a single down-to-the-west normal fault (F1; T2S meter marks 9.3, 0.3; plate 1) with shear fabric in a zone as much as 20 cm wide (e.g., T2S meter marks 9, 1; plate 1); in the north wall, the fault splays into two distinct down-to-the-west strands (plate 1). In the south wall, the shear zone also contains two main antithetic normal faults (F2; T2S meter marks 9.5, 0.2; and F3; T2S meter marks 10.5, 0.1; plate 1), several minor subsidiary faults and fractures, and a steeply dipping antithetic reverse fault (F4; T2S meter marks 13, 1.0; plate 1). The main fault's (F1) strike and dip are 193°/80° NW, but the dip decreases to 65°–75° near the base of the wall. Subsidiary faults and fractures dip 65°–80° NW and 66°–86° SE; however, most dip 75°–80° NW. We mapped a soil- and fan-alluvium-filled fissure in the south wall (T2S meter marks 10.5, 2.5; plate 1) that opened along antithetic fault F3. The fissure is a maximum of 70 cm wide and tapers downward, terminating at about mid-height in the south wall (T2S meter marks 10.5, 1.8; plate 1). Most faults and fractures exposed in the trench continue from the base of the trench up to within units 6 and 7 of T2S, where their traces become indistinct. We infer that apparent fault and fracture terminations at the 2-m-wide bench between the two vertical walls comprising the south wall (e.g., F4a and F4b; T2S meter marks 12.5–13.5, 1.2; plate 1) are the result of the complex structure of the fault zone, including changes in fault orientation and number of splays and the width of the bench.

The vertical displacement of units mapped on both sides of the fault zone ranges from 2.7 to 3.3 m (average of 3.0 m; table 5). This is similar to the far-field surface offset of 2.5–3.0 m based on a long GPS profile (GPS profile 1; figures 5 and 7; plate 1), a shorter GPS profile (GPS profile 6; figure 5; plate 1), and profiles P32 and P34 measured by DuRoss (2004) (plate 1). Vertical-displacement estimates for the two antithetic faults are 40–50 cm per fault, whereas the other subsidiary faults have less than 20 cm of displacement.

Table 5. *Net vertical displacement of alluvial-fan units in the Santaquin trenches*

Contact[1]	Trench 1 (m)[2]	Trench 2 (m)[2]
1-2	**3.1**	-
2-3	**3.1**	**2.9**
3-4	3.0	**3.2**
4-5	2.8	3.3
5-6	-	**3.1**–3.2
6-7	-	2.7
7-8	**2.8**	-
Average displacement[3]	**3.0 ± 0.2**	**3.0 ± 0.2**
Surface offset[4]	2.2–3.3	2.5–3.0
Preferred[5]	**3.0 ± 0.2**	

[1]Unit contacts, as mapped from trench 1 north wall and trench 2 south wall (plate 1).
[2]Values are vertical separation of unit contacts projected toward the main fault on the trench logs; bold indicates data of best quality.
[3]Average displacement (± one standard deviation), based on measured stratigraphic displacements; for unit 5-6 contact, bold value was used in average calculation.
[4]Surface offset based on projection of far-field surface slopes toward scarp midpoint. Values represent range of mean offset values from laser-range-finder (DuRoss, 2004) and precision-grade-GPS scarp profiles 1 and 2 (figure 5; plate 1).
[5]Preferred vertical displacement ± one standard deviation for Santaquin trench site.

RESULTS OF INVESTIGATION

Number of Earthquakes

Our trenches at Santaquin exposed evidence for a single surface-faulting earthquake (figure 10). In both trench exposures we mapped scarp-derived colluvial wedges associated with the MRE, and in trench 2 we inferred that a fissure opened along an antithetic fault during the most recent surface-faulting event. In both trenches we correlated faulted alluvial-fan deposits buried by the scarp colluvium with deposits in both the hanging wall and footwall of the fault zones. Additionally, net vertical stratigraphic displacements (2.7–3.2 m) are similar to scarp-profile-displacement estimates (2.2–3.3 m) and are twice the maximum thickness of the colluvial wedge (1.5 m) in trench 2, consistent with mass-volume (scarp erosion-deposition) calculations. Also, in trench 2, the north and south walls exposed remarkably different geometries for the colluvial wedges, but we estimated similar areas for both exposures (2.5–3.0 m^2 and 2.7–3.2 m^2, respectively). These estimates are comparable to our 2.8–4.2 m^2 estimate for material eroded from the crest of the fault scarp and support just a single earthquake. Subsidiary faults and fractures in the trenches also support a single earthquake hypothesis. We found no consistent increase in displacement with deposit age (i.e., differential displacement indicating multiple faulting events). Most faults and fractures terminate within the youngest deposits faulted by the MRE, and no faults penetrate deposits mapped as fault-scarp colluvium.

Earthquake Timing

Most Recent Earthquake

Constraints on the timing of the MRE at the Santaquin site are primarily based on dated charcoal or soil organics from the trench 2 south-wall exposure (plate 1). There, we mapped a well-developed soil on alluvial-fan deposits (unit 7) faulted down to the northwest and buried by a scarp-derived colluvial wedge (unit 8). Aggregated charcoal fragments from two different bulk soil samples collected from below the colluvial wedge yielded maximum-limiting times for the MRE of 500 ± 50 and 550 ± 50 cal yr B.P. Charcoal fragments from an organic stringer within the scarp colluvium constrain the earthquake timing to a minimum of 425 ± 125 cal yr B.P. (table 4). In the north wall of trench 2, the MRE also postdates a 1500 cal yr B.P. soil formed within alluvial-fan deposits faulted by the event. However, since an unknown amount of time elapsed between soil burial and MRE faulting (during which a debris flow was deposited), the age is a poor maximum constraint on the timing of the MRE. We also obtained an erroneous 6600 cal yr B.P. age for an MRE fissure-fill deposit (unit 8a) in the trench 2 south wall. We interpret the unexpectedly old age as having a significant inherited component from detrital charcoal.

We were unable to use ages of charcoal and bulk-soil samples from trench 1 to constrain timing of the MRE. In both the north- and south-wall exposures, a post-faulting debris flow (units 9 and 6, respectively; figure 10) has obscured and buried the scarp colluvium (units 8 and 5, respectively; figure 10), and no buried soil exists below the colluvium. Radiocarbon ages on charcoal fragments collected from the base of the post-faulting debris flow are anomalously old as the fragments sampled and dated are likely reworked (i.e., detrital), having a significant inherited age. In addition, we interpret the 9400 cal yr B.P. age from detrital charcoal in the youngest faulted deposit (unit 7) in trench 1 as being mostly an inherited age.

The Santaquin MRE must have occurred between 425 and 550 cal yr B.P., based on the midpoints of the calendar-calibrated radiocarbon ages. However, since the faulted soil was likely buried rapidly after the surface-faulting event, and an unknown span of time elapsed during which soil organics accumulated within the scarp colluvium, we conclude that the earthquake occurred near the older end of the maximum-limiting time range (i.e., closer to 550 than 425 years). Further, we used OxCal radiocarbon calibration and analysis software (version 3.10; Bronk Ramsey, 1995, 2001, 2006; using the IntCal04 calibration curve of Reimer and others, 2004), which integrates calendar-calibrated age distributions, stratigraphic ordering, and conditional probabilities to model the age distribution of an undated event, to determine an earthquake time of 480 cal yr B.P. (modal value) with a two-sigma time range of 330–550 cal yr B.P. (480 +70/-150 cal yr B.P.) (figure 11). Thus, considering both estimates and rounding to the nearest half or full century, we report a Santaquin MRE timing estimate (± two sigma) of 500 +100/-150 cal yr B.P.

Penultimate Earthquake

We found no structural or stratigraphic evidence (e.g., fault terminations or differential displacement) for an older (penultimate) surface-faulting paleoearthquake (P2) in the trench exposures. Additionally, the simple fault-scarp geometry and geomorphology at the site (e.g., no older or larger scarps are present on other parts of the alluvial fan) support a P2 event that predates most of the alluvial-fan deposits. Thus, we can only infer a minimum time since the event using dated alluvial-fan deposits in the trenches.

P2 must predate the oldest alluvial-fan deposits exposed in both trenches. In trench 1, P2 must predate T1N unit 2, as the unit 1-2 contact exposed near the base of the hanging-wall exposure has a similar displacement as the unit 7-8 contact below the colluvial wedge (table 5). We were unable to date T1N unit 2, but radiocarbon-dated detrital charcoal (STRC-18; table 4) from the top of T1N unit 3, collected from near the base of the hanging wall, yielded an age of 6900 (6800–7000; 2-sigma range) cal yr B.P. Given difficulties with inherited ages obtained from other trench 1 samples (e.g., STRC-16; table 4), we recognize that the 6900-year age may have an unknown inherited-age component. In trench 2, P2 predates T2S unit 3, which is not displaced significantly more than the youngest deposits below the colluvial wedge (T2S units 6 and 7; plate 1). We did not obtain ages for T2S units 2 through 6; however, near the base of the footwall exposure, we dated detrital charcoal (STRC-14; table 4) entrained in T2S unit 1 at 8600 (8500–8700) cal yr B.P. T2S unit 1 is not exposed on the hanging wall, thus this age cannot be used to constrain P2 timing. P2 also predates T2N unit 3, exposed in the trench 2 north wall. Radiocarbon-dated charcoal separated from a buried soil within the unit indicates an age of 1500 cal yr B.P., which is a poor minimum constraint on P2 timing. Thus, we infer that P2 must

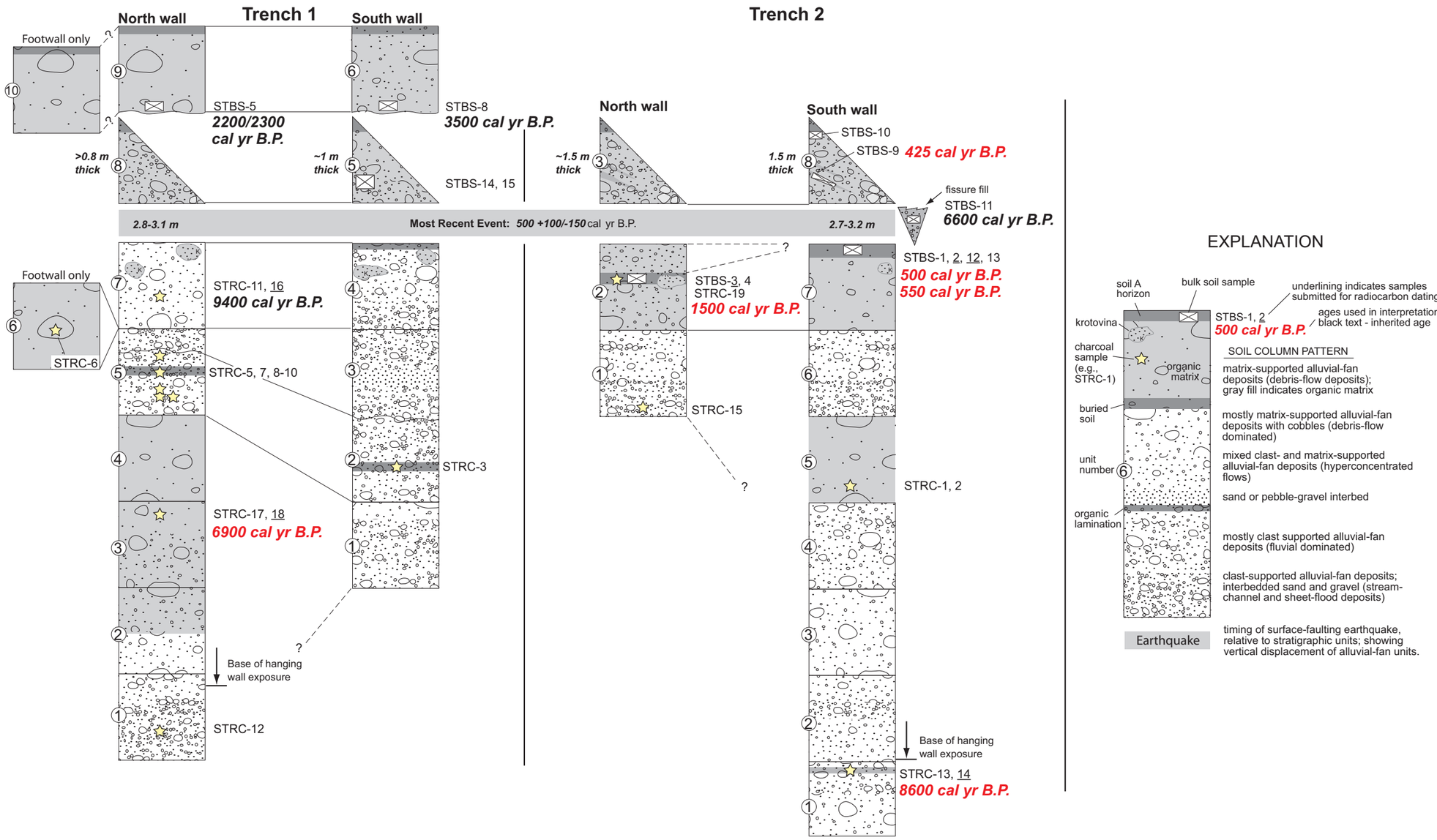

Figure 10. *Correlation of alluvial-fan deposits (boxes) and scarp colluvium (triangles) exposed in the Santaquin fault trenches, showing MRE preferred timing and vertical displacement estimates. Calendar-calibrated ages (midpoint of 2-standard-deviation range) used in interpretation of earthquake timing shown in red.*

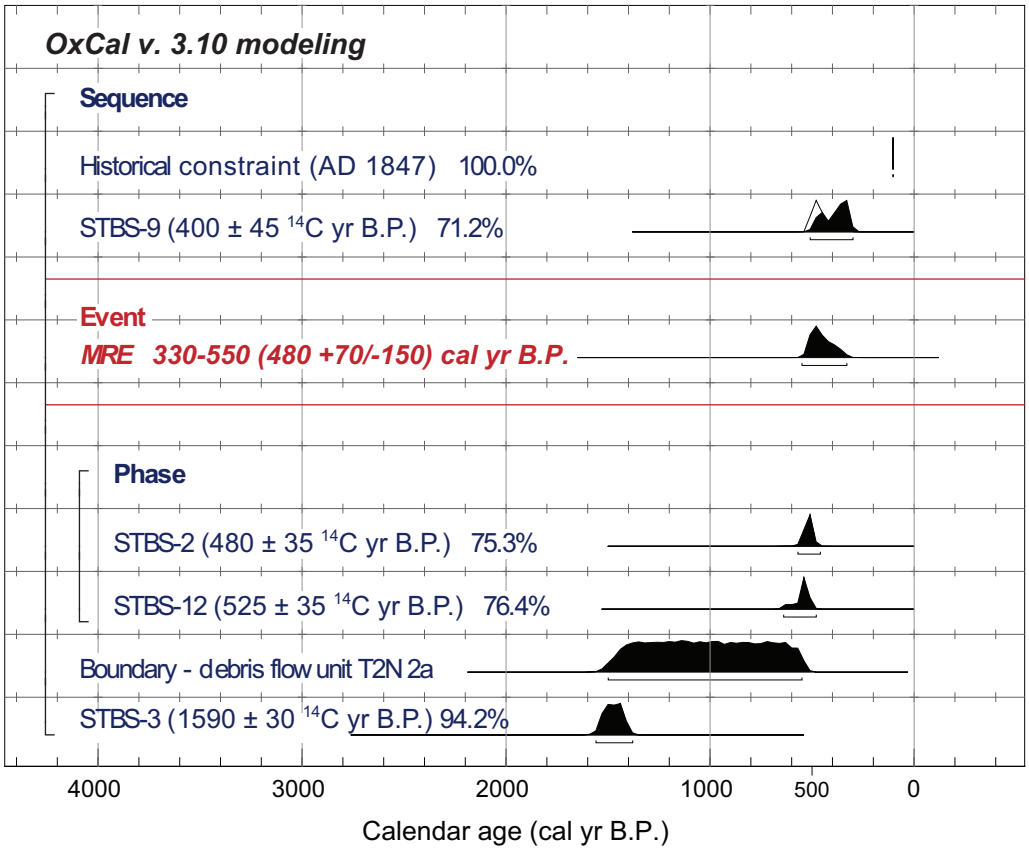

Figure 11. *Stratigraphic ordering and numerical control using OxCal v. 3.10 (Bronk Ramsey, 2005), showing probability density functions for radiocarbon ages (table 4) and the modeled Santaquin MRE with 2-sigma age range (330–550 cal yr B.P.) and modal value (480 cal yr B.P.). Unshaded areas represent prior (pre-modeling) distributions using atmospheric data from Reimer and others (2004); shaded (black) areas indicate posterior (modeled) distributions using stratigraphic ordering information. Horizontal bars below distributions show two-sigma age ranges for posterior distributions; percentages indicate degree of overlap between prior and posterior distributions.*

have occurred before 1500 cal yr B.P. and likely occurred before 6800–7000 cal yr B.P.

Vertical Displacement

Our preferred vertical displacement for the MRE at the Santaquin trench site is 3.0 ± 0.2 m, based on the mean of 10 stratigraphic-displacement measurements of alluvial-fan-unit contacts exposed in both trenches. This displacement value corresponds well with scarp-profile offset measurements of 2.2–3.3 m near trench 1 and 2.5–3.0 m near trench 2 (table 5; plate 1). Also, the displacement measurement lacks complicating P2 displacement and is reasonable for a single event given the scarp height and offset measurements and maximum thickness of the colluvial wedge in trench 2. If the 3-m displacement occurred during a single earthquake, we would expect an approximately 3-m-high scarp (because of the simple fault geometry and gentle surface slope) and a maximum colluvial-wedge thickness of about half the scarp height (i.e., 1.5 m) (Ostenaa, 1984). The trench 2 colluvial-wedge exposures, which each had a maximum thickness of 1.5 m (plate 1), support this scenario. We did not consider the trench 1 colluvial-wedge thickness because a post-event debris flow has modified or obscured part of the wedge (figure 9a; plate 1).

Slip Rate and Recurrence Interval

We have evidence only for the MRE at the Santaquin site, and thus cannot accurately measure fault slip rate based on a closed seismic interval, that is, the time interval between two dated paleoearthquakes. However, we calculated a longer-term geologic vertical slip rate of 0.5 mm/yr at the site using 9 m of Bonneville-shoreline-elevation change across the WFZ (discussed above under "Geologic Setting") and the timing of Bonneville-shoreline abandonment at 16,800 cal yr B.P. Although 0.5 mm/yr is a reasonable (but low) Holocene slip-rate estimate for the WFZ at the Santaquin site, the rate is not a well-constrained, seismic-interval-based rate because an unknown amount of time elapsed between shoreline abandonment at 16,800 cal yr B.P. and the first post-Bonneville (>7000 years?) surface-faulting earthquake at the site. However, the slip rate corresponds well with the 0.5 mm/yr estimate for the northern strand by DuRoss and Bruhn (2005) based on scarp-profile displacements and diffusion-modeling-based earthquake timing. In comparison, the Utah Quaternary Fault Parameters Working Group (UQFPWG; Lund, 2005) reports a consensus Holocene slip-rate estimate (minimum-preferred-maximum) based on the then-best-available data for the Nephi segment of 0.5-1.1-3.0 mm/yr.

By dividing our vertical displacement of 3.0 ± 0.2 m measured in the Santaquin trenches by the longer-term slip

rate (0.5 mm/yr), we estimate an average recurrence interval between surface-faulting earthquakes of 5600–6400 years. This recurrence-interval estimate is considerably longer than previously reported average estimates for the southern part of the Nephi segment of about 2700 and 2500 years (McCalpin and Nishenko, 1996, and Lund, 2005, respectively), longer than the 2100–4100-year estimate of DuRoss and Bruhn (2005), and greater than the upper end of the estimated two-sigma range (1200–4800 years) reported by the UQFPWG (Lund, 2005). Using our average recurrence-interval estimate and the 500 cal yr B.P. MRE timing, the penultimate event may have occurred between 6100 and 6900 cal yr B.P., which is close to but mostly younger than the 6800–7000 cal yr B.P. minimum-time estimate for P2 based on radiocarbon samples from the Santaquin trenches.

Paleoearthquake Magnitude and Surface Rupture Length

Determining magnitude estimates for paleoearthquakes requires knowledge of fault-rupture parameters (e.g., surface rupture length [SRL] and/or maximum or average vertical displacement [VDmax or VDavg]) for comparison with empirical fault-parameter-magnitude regressions (e.g., Tocher, 1958; Slemmons, 1977; Bonilla and others, 1984; Wells and Coppersmith, 1994). We estimated the magnitude of surface-faulting earthquakes on the Nephi segment by comparing the Santaquin-site fault-rupture parameters to the all-fault-type SRL-magnitude and vertical-displacement-magnitude regressions of Wells and Coppersmith (1994), and to the seismic-moment-magnitude conversion of Hanks and Kanamori (1979). Because the total rupture length of the Santaquin MRE is unknown, we used a minimum value equal to the length (straight-line distance) of the northern strand of the Nephi segment (17 km; figure 1) and a maximum value equal to the full length of the Nephi segment (42 km; figure 1). For displacement estimates, we used our 3-m displacement from the Santaquin site as both a possible maximum and average displacement, and a 4-m estimate based on scarp profiles from the southern part of the northern strand (DuRoss, 2004) as a second possible maximum.

Our moment-magnitude (Mw) estimate for the Santaquin MRE is 7.0 ± 0.3, based on four different SRL and vertical-displacement empirical regressions (table 6). The magnitude uncertainty reflects lower Mw estimates from SRL regressions (6.5–7.0) than from vertical-displacement regressions (7.0–7.3). Estimates of Mw based on regressions that use both vertical displacement and SRL (6.8–6.9 using a 3-m displacement and 17-km-long SRL, and 7.0–7.1 using a 3-m displacement and 42-km-long SRL) fall between the separate SRL- and vertical-displacement-based estimates (table 6). The large uncertainty in the Santaquin MRE SRL results in considerably different estimates of seismic moment release. The moment-magnitude scale of Hanks and Kanamori (1979; table 2) estimates about 2.5 times more energy for an earthquake having a vertical displacement of 3 m and SRL of 42 km (8.1×10^{26} dyne-cm) than for an earthquake having an identical vertical displacement but SRL of 17 km (3.3×10^{26} dyne-cm).

Table 6 illustrates a significant discrepancy between magnitude estimates based on the 17-km-long length of the northern strand (6.5–6.9) and those based on a 3-m displacement estimate (7.0–7.3). Although 3 m is a considerable net displacement for the WFZ (table 1), we do not consider it to be a maximum value because scarps of similar size and vertical separation are present on the northern strand both to the north and south of the Santaquin site (Machette, 1992; DuRoss and Bruhn, 2005; D. Horns, Utah Valley State College, verbal communication, 2006).

Table 6. *Moment-magnitude estimates for the most recent surface-faulting earthquake at the Santaquin site on the Nephi segment.*

Earthquake Parameter[1]		Moment Magnitude (M_w)
SRL[2]	17 km	6.5
SRL[2]	42 km	7.0
VD_{max}[2]	3.0 m	7.0
VD_{max}[2]	4.0 m	7.1
VD_{avg}[2]	3.0 m	7.3
SRL, VD_{avg}, A[3]	17 km, 3 m, 333 km^2	6.8–6.9 (6.8)[4]
SRL, VD_{avg}, A[3]	42 km, 3 m, 822 km^2	7.0–7.1 (7.1)[4]
Mean +/- one standard deviation:		**7.0 ± 0.3**[4]

[1] SRL – surface rupture length, VD_{max} – maximum vertical displacement, VD_{avg} – average vertical displacement, A – fault-rupture-plane area (SRL multiplied by down-dip rupture width).

[2] All-fault-type relations (from Wells and Coppersmith, 1994): $M_w = 1.16 \log SRL + 5.08$; $M_w = 0.74 \log VD_{max} + 6.69$; $M_w = 0.82 \log VD_{avg} + 6.93$.

[3] Based on Hanks and Kanamori (1979), where seismic moment (M_o) = $\mu\, VD_{avg}\, A$, and $M_w = 0.66 \log M_o - 10.7$; μ is shear modulus. We assume that $\mu = 3.3 \times 10^{11}$ dyne/cm^2, fault dip = 50 ± 10 degrees, and seismogenic depth = 15 km.

[4] The magnitude range reflects fault dips of 40 and 60 degrees; the value in parentheses is based on a fault dip of 50 degrees and is used to calculate the mean magnitude estimate.

Using the method of Biasi and Weldon (2006), we estimated the likelihood of a minimum SRL given an observed displacement of 3 m (assumed to be randomly sampled along the fault, and representing an average value): it is 95% likely that the Santaquin MRE had a SRL of at least 50 km. This estimate is considerably longer than the mapped length of the northern strand (17 km), and close to but even longer than the entire length of the Nephi segment (42 km). Thus, we consider it unlikely that the Santaquin earthquake occurred only on the northern strand as a partial-segment rupture, but rather infer that surface faulting at the Santaquin site occurred either (1) as part of the rupture of the entire Nephi segment at about 300 years ago (Machette and others, 2007), or (2) as part of the MRE rupture on the 59-km-long Provo segment at approximately 500-600 cal yr B.P. (Machette and others, 1992; Lund, 2005). Resolving whether (1) or (2) above is true requires comparing the Santaquin MRE parameters with those currently being developed for the Provo segment (S. Olig, URS Corporation, verbal communication, 2006) and southern strand of the Nephi segment (Willow Creek site; U.S. Geological Survey), and with existing paleoseismic information for the Provo, Nephi, and Levan segments (Lund, 2005).

Summary

We excavated two trenches across the WFZ near Santaquin, Utah, and exposed evidence for a single surface-faulting earthquake that displaced alluvial-fan deposits and a fan-surface soil 3.0 ± 0.2 m down-to-the-northwest at about 500 +100/-150 cal yr B.P. (table 7). We mapped scarp-derived colluvial-wedge deposits that locally buried the faulted alluvial-fan surface and its soil. Radiocarbon ages from charcoal collected from the fan-surface soil below the colluvial wedge constrain timing of the event to a maximum of 500–550 cal yr B.P. Radiocarbon-dated charcoal from an organic stringer contained within the wedge colluvium provides a minimum time since the earthquake of 425 ± 125 cal yr B.P. Considering the observed displacement measurement of 3.0 ± 0.2 m, we estimate that the Santaquin MRE had an SRL of at least 42 km (based on the entire length of the Nephi segment) and possibly as great as 50 km (using the method of Biasi and Weldon, 2006), and thus consider it unlikely that the event was limited to the 17-km-long northern strand of the Nephi segment. Comparison of SRL and estimates of VDmax and VDavg with empirical fault-parameter-magnitude regressions results in an estimated moment magnitude of 7.0 ± 0.3.

We report a longer-term geologic vertical slip rate of 0.5 mm/yr based on 9 m of displacement across the Bonneville shoreline (abandoned at 16,800 years), which we estimated from a GPS survey. This rate corresponds with the minimum Holocene slip-rate estimate of the UQFPWG (Lund, 2005) and the northern-strand slip-rate estimate based on fault-scarp diffusion modeling by DuRoss and Bruhn (2005). We determined an average recurrence interval between surface-faulting earthquakes of 5600–6400 years by dividing our displacement measurement (2.8–3.2 m) by the longer-term slip rate (table 7). Our recurrence-interval estimate is longer than estimates based on previously existing paleoseismic data (1200–4800 years; Lund, 2005) and fault-scarp diffusion modeling for the northern strand (2100–4100 years; DuRoss and Bruhn, 2005).

We found no structural or stratigraphic evidence for P2 in the trench exposures, and thus were unable to closely constrain the timing of the earthquake. However, using radiocarbon-dated samples from the oldest hanging-wall deposits in the Santaquin trenches, and the MRE timing and average recurrence interval, we estimate a poorly constrained minimum time of 6100-7000 cal yr B.P. for P2.

CONCLUSIONS AND IMPLICATIONS FOR SEGMENTATION

Paleoseismic data from the Santaquin trench site support the proposition of DuRoss and Bruhn (2005) that the northern and southern strands of the Nephi segment may behave independently. Our new data show that both strands have evidence for Holocene surface-faulting earthquakes, but considerably different Holocene earthquake chronologies and rates of activity. At the Santaquin site, a singe earthquake at 500 +100/-150 cal yr B.P occurred in the past 6100–7000 years, which corresponds with a low post-Bonneville-shoreline (17-ka) slip rate of 0.5 mm/yr. In contrast, the southern strand has good evidence for three earthquakes since the mid-Holocene (Hanson and others, 1981; Jackson, 1991; Lund, 2005), and preliminary results from the Willow Creek site suggest three large-magnitude earthquakes since 2320 cal yr B.P., with the youngest event at about 300 cal yr B.P. (Machette and others, 2007). These new data yield an average minimum slip rate of 2.0–2.5 mm/yr, based on 4–5 m of displacement in the 2000-year interval between the first and third events at the site (Machette and others, 2007). Thus, the unique earthquake histories and disparate rates of

Table 7. *Summary of Santaquin trench site paleoseismology*[1].

Earthquake	Timing (cal yr B.P.)	VD (m)	Magnitude	SRL (km)	ARI (yr)	Longer-term SR (mm/yr)
MRE (Z)	500 +100/-150	3.0 ± 0.2	7.0 ± 0.3	42–50 km	5600–6400	0.5
P2 (Y)	>6100–7000	-	-	-		

[1] See text for discussion of earthquake parameters and uncertainties. Abbreviations are as follows: MRE – most recent event, P2 – second paleoearthquake, VD – vertical displacement, SRL – surface rupture length, ARI – average recurrence interval (VD divided by the longer-term slip rate [SR]).

activity of the northern and southern strands of the Nephi segment indicate they have behaved independently since at least the mid-Holocene.

The 500-year MRE interpreted from the Santaquin paleoseismic data likely represents the tail-end of surface rupture associated with a large surface-faulting earthquake. Surface faulting at the Santaquin site probably occurred contemporaneously with a large (SRL greater than 42–50 km) earthquake on either the southern strand of the Nephi segment or the Provo segment, rather than during a separate earthquake limited only to the northern strand. This inference is supported by the short (17 km) length of the northern strand, the large (3 m) displacement for the Santaquin MRE (which suggests an SRL greater than 50 km), and a Santaquin MRE timing that is comparable to the youngest events on the southern Nephi strand and Provo segment. The two-sigma time range for the northern strand MRE is 350–600 cal yr B.P., based on the Santaquin data, which is close to the 300-year estimate for the southern-strand MRE from the Willow Creek site. However, two additional events identified at Willow Creek at approximately 1200 and 2300 years did not rupture the Santaquin site. Paleoseismic data for the Provo segment suggest MRE timing of about 500–600 years (Machette and others, 1992; Lund and Black, 1998; Lund, 2005), and new data from a paleoseismic investigation near Mapleton (Olig and others, 2004) suggest MRE timing near the younger end of the range (500 ± 150 cal yr B.P.; Olig, URS Corp., verbal communication, 2006). However, additional late Holocene events on the Provo segment at about 1600 and 2850 cal yr B.P. (Lund, 2005; Olig, verbal communication, 2006) are absent from the Santaquin-site record. Our preferred scenario includes the northern strand MRE as part of a large surface-faulting earthquake on the Provo segment at about 500 cal yr B.P. However, given the disparate rates of activity between the northern strand and Provo segment, this case of spill-over rupture may be exceptional.

Although the northern strand is defined as part of the Nephi segment, based on a bedrock fault that connects the two strands, its low rate of activity during the Holocene may be related to the relatively more active Provo segment. The decreased frequency of earthquakes on the northern strand of the Nephi segment (i.e., average recurrence of 6000 years as opposed to approximately 1000 years on the southern strand) may be due to stress relaxation along the northern part of the Nephi segment. For example, a shadow effect would occur east and west of the Provo segment following a large-magnitude, Provo segment earthquake (Chang and Smith, 2002). This area of relaxed stress corresponds with the northern part of the Nephi segment, which overlaps with the southernmost Provo segment (figure 1) (DuRoss and Bruhn, 2005), and may explain the decreased rates of activity on the northern strand. Additionally, spill-over rupture from the Provo segment to the northern Nephi segment would release strain accumulated over thousands of years (considering the low 0.5 mm/yr slip rate) on the northern strand. Both of these processes may contribute to a decrease in the probability of rupture propagation from the southern to northern strands of the Nephi segment.

To resolve these segmentation issues, re-evaluations are necessary of the timing of the MRE on (1) the southern strand of the Nephi segment, using North Creek, Red Canyon, and Willow Creek paleoseismic data, and (2) the Provo segment, using new paleoseismic data from the Mapleton site and unpublished data (ca. 1987) from U.S. Bureau of Reclamation trenches excavated on the southernmost part of the Provo segment (see Machette and others, 1992). Ultimately, re-evaluated earthquake chronologies and refined models of segmentation for the Nephi and Provo segments are key components of understanding the past (Holocene) and future behavior of the WFZ, improving WFZ hazard models, and reducing Utah's earthquake-related risk.

ACKNOWLEDGMENTS

This work was supported by the U.S. Geological Survey National Earthquake Hazards Reduction Program (award no. 05HQGR0098) and the Utah Geological Survey; the U.S. Forest Service (Matthew Keyes and Duane Resare, Uinta National Forest, Spanish Fork Ranger District) granted land access. We thank Gary Christenson, Rich Giraud, Mike Hylland, and Michael Kirschbaum (UGS), Michael Machette, Anthony Crone, and Stephen Personius (USGS), and Susan Olig (URS Corp.) for discussions of this work and assistance in the field. Gary Christenson, Mike Hylland, and Michael Machette provided helpful review comments.

REFERENCES

Andrews, D.J., and Bucknam, R.C., 1987, Fitting degradation of shoreline scarps by a nonlinear diffusion model: Journal of Geophysical Research, v. 92, no. B12, p. 12,857-12,867.

Bennett, R.A., Wernicke, B.P., Niemi, N.A., Friedrich, A.M., and Davis, J.L., 2003, Contemporary strain rates in the northern Basin and Range Province from GPS data: Tectonics, v. 22, no. 2, 29 p.

Biasi, G.P., and Weldon, R.J., 2006, Estimating surface rupture length and magnitude of paleoearthquakes from point measurements of rupture displacement: Bulletin of the Seismological Society of America, v. 96, no. 5, p. 1612-1623.

Birkeland, P.W., Machette, M.N., and Haller, K.M., 1991, Soils as a tool for applied Quaternary geology: Utah Geological and Mineral Survey Miscellaneous Publication 91-3, 63 p.

Black, B.D., Hecker, S., Hylland, M.D., Christenson, G.E., and McDonald, G.N., 2003, Quaternary fault and fold database and map of Utah: Utah Geological Survey Map 193DM, scale 1:500,000, compact disk.

Bolt, B.A., 1999, Earthquakes, fourth edition: New York, W.H. Freeman and Company, 366 p.

Bonilla, M.G., Mark, R.K., and Lienkaemper, J.J., 1984, Statistical relations among earthquake magnitude, surface rupture length, and surface fault displacement: Bulletin of the Seismological Society of America, v. 74, p. 2379-2411.

Bronk Ramsey, C., 1995, Radiocarbon calibration and analysis of stratigraphy – the OxCal program: Radiocarbon, v. 37, no. 2, p. 425-430.

Bronk Ramsey, C., 2001, Development of the radiocarbon program OxCal: Radiocarbon, v. 43, no. 2A, p. 355-363.

Bronk Ramsey, C., 2006, OxCal program version 3.10, Radiocarbon Accelerator Unit: Oxford, United Kingdom, University of Oxford, online, <http://www.rlaha.ox.ac.uk/ oxcal/ oxcal.htm>, accessed May 2006.

Bucknam, R.C., 1978, Northwestern Utah seismotectonics studies, *in* Seiders, W., and Thomson, J., compilers, Summaries of technical reports, v. VII: Menlo Park, California, U.S. Geological Survey Office of Earthquake Studies, p. 64.

Chang, W.L., and Smith, R.B., 2002, Integrated seismic-hazard analysis of the Wasatch Front, Utah: Bulletin of the Seismological Society of America, v. 92, no. 5, p. 1904-1922.

Chang, W.L., Smith, R.B., Meertens, C.M., and Harris, R.B., 2006, Contemporary deformation of the Wasatch fault, Utah, from GPS measurements with implications for interseismic fault behavior and earthquake hazard – observations and kinematic analysis: Journal of Geophysical Research, vol. 111, 19 p.

dePolo, C.M., Clark, D.G., Slemmons, D.B., and Ramelli, A.R., 1991, Historical surface faulting in the Basin and Range Province, western North America – implications for fault segmentation: Journal of Structural Geology, v. 13, no. 2, p. 123-136.

DuRoss, C.B., 2004, Spatial and temporal trends of surface rupturing on the Nephi segment of the Wasatch fault, Utah – implications for fault segmentation and the recurrence of paleoearthquakes: Salt Lake City, University of Utah, M.S. thesis, 120 p.

DuRoss, C.B., 2006, The potential for multi-segment rupture on the central segments of the Wasatch fault zone, Utah, *in* Christenson, G.E., DuRoss, C.B., Hylland, M.D., Lund, W.R., and McDonald, G.N., Earthquake working groups, database updates, and paleoseismic fault studies, Utah: Utah Geological Survey, Final Technical Report to the U.S. Geological Survey, National Earthquake Hazards Reduction Program, award no. 03HQAG0008, 24 p., compact disk.

DuRoss, C.B., and Bruhn, R.L., 2005, Active tectonics of the Nephi segment, Wasatch fault zone, Utah, *in* Lund, W.R., editor, Western States Seismic Policy Council Proceedings Volume of the Basin and Range Province Seismic Hazards Summit II: Utah Geological Survey Miscellaneous Publication 05-2, 25 p., compact disk.

Felger, T.J., Machette, M.N., and Sorensen, M.L., 2004, Provisional geologic map of the Mona quadrangle, Juab and Utah Counties, Utah: Utah Geological Survey Open-File Report 428, 23 p., 2 plates, scale 1:24,000.

Giraud, R.E., 2005, Guidelines for the geologic evaluation of debris-flow hazards on alluvial fans in Utah: Utah Geological Survey Miscellaneous Publication 05-6, 16 p.

Hanks, T.C., and Kanamori, H., 1979, A moment magnitude scale: Journal of Geophysical Research, v. 84, no. B5, p. 2348-2350.

Hanson, K.L., Swan, F.H., and Schwartz, D.P., 1981, Study of earthquake recurrence intervals on the Wasatch fault, Utah: San Francisco, California, Woodward-Clyde Consultants, sixth annual technical report prepared for U.S. Geological Survey under contract no. 14-08-0001-19115, 22 p.

Hanson, K.L., Swan, F.H., and Schwartz, D.P., 1982a, Study of earthquake recurrence intervals on the Wasatch fault, Utah: San Francisco, California, Woodward-Clyde Consultants, seventh annual technical report prepared for U.S. Geological Survey under contract no. 14-08-0001-19842, 10 p.

Hanson, K.L., Swan, F.H., and Schwartz, D.P., 1982b, Guidebook to late Pleistocene and Holocene faulting along the Wasatch Front and vicinity – Little Cottonwood Canyon to Scipio, Utah, *in* Hanson, K.L., and Schwartz, D.P., editors, Proceedings of the American Geophysical Union Chapman Conference on Fault Behavior and the Earthquake Generation Process, Snowbird, Utah, 40 p.

Harty, K.M., Mulvey, W.E., and Machette, M.N., 1997, Surficial geologic map of the Nephi segment of the Wasatch fault zone, eastern Juab County, Utah: Utah Geological Survey Map 170, 14 p., 1 plate, scale 1:50,000.

Hylland, M.D., and Machette, M.N., 2004, Interim surficial geologic map of the Levan segment of the Wasatch fault zone, Juab and Sanpete Counties, Utah, *in* Christenson, G.E., Ashland, F.X., Hylland, M.D., McDonald, G.N., and Case, B., Database compilation, coordination of earthquake hazards mapping, and study of the Wasatch fault and earthquake induced landslides, Wasatch Front, Utah: Utah Geological Survey Final Technical Report to the U.S. Geological Survey, National Earthquake Hazards Reduction Program, award no. 03HQAG0008, 30 p., scale 1:50,000, compact disk.

Hylland, M.D., and Machette, M.N., in press, Surficial geologic map of the Levan and Fayette segments of the Wasatch fault zone, Juab and Sanpete Counties, Utah: Utah Geological Survey Map, scale 1:50,000.

Jackson, M., 1991, Paleoseismology of Utah, Volume 3 – Number and timing of Holocene paleoseismic events on the Nephi and Levan segments, Wasatch fault zone, Utah: Utah Geological Survey Special Study 78, 23 p.

Lund, W.R., 2005, Consensus preferred recurrence-interval and vertical slip-rate estimates – review of Utah paleoseismic-trenching data by the Utah Quaternary Fault Parameters Working Group: Utah Geological Survey Bulletin 130, 109 p., compact disk.

Lund, W.R., and Black, B.D., 1998, Paleoseismology of Utah, Volume 8 - Paleoseismic investigation at Rock Canyon, Provo segment, Wasatch fault zone, Utah County, Utah: Utah Geological Survey Special Study 93, 21 p.

Machette, M.N., 1992, Surficial geologic map of the Wasatch fault zone, eastern part of Utah Valley, Utah County and parts of Salt Lake and Juab Counties, Utah: U.S. Geological Survey Miscellaneous Investigations Series Map I-2095, scale 1:50,000, 30 p. pamphlet.

Machette, M.N., Crone, A.J., Personius, S.F., Mahan, S.A., Dart, R.L., Lidke, D.J., and Olig, S.S., 2007, Paleoseismology of the Nephi segment of the Wasatch fault zone, Juab County, Utah – Preliminary results from two large exploratory trenches at Willow Creek: U.S. Geological Survey Scientific Investigations Map SI-2966, 2 plates.

Machette, M.N., Personius, S.F., and Nelson, A.R., 1992, Paleoseismology of the Wasatch fault zone – a summary of recent investigations, interpretations, and conclusions, *in* Gori, P.L., and Hays, W.W., editors, Assessment of regional earthquake hazards and risk along the Wasatch Front, Utah: U.S. Geological Survey Professional Paper 1500-A, p. A1-A71.

Mattson, A., and Bruhn, R.L., 2001, Fault slip rates and initiation age based on diffusion equation modeling – Wasatch fault zone and eastern Great Basin: Journal of Geophysical Research, v. 106, no. B7, p. 13,739–13,750.

McCalpin, J.P., editor, 1996, Paleoseismology: San Diego, Academic Press, 588 p.

McCalpin, J.P., 2002, Paleoseismology of Utah, Volume 10 – Post-Bonneville paleoearthquake chronology of the Salt Lake City segment, Wasatch fault zone, from the 1999 "Megatrench" site: Utah Geological Survey Miscellaneous Publication 02-7, 37 p.

McCalpin, J.P., and Forman, S.L., 2002, Paleoseismology of Utah, Volume 11 – Post-Provo paleoearthquake chronology of the Brigham City segment, Wasatch fault zone, Utah: Utah Geological Survey Miscellaneous Publication 02-9, 46 p.

McCalpin, J.P., Forman, S.L., and Lowe, M., 1994, Reevaluation of Holocene faulting at the Kaysville site, Weber segment of the Wasatch fault zone, Utah: Tectonics, v. 13, no. 1, p. 1-16.

McCalpin, J.P., and Nishenko, S.P., 1996, Holocene paleoseismicity, temporal clustering, and probabilities of future large (M > 7) earthquakes on the Wasatch fault zone, Utah: Journal of Geophysical Research, v. 101, no. 3, p. 6233-6253.

National Aeronautics & Space Administration (NASA), 2006, Visible Earth – a catalog of NASA images and animations of our home planet: Online, <http://visibleearth.nasa.gov/>, accessed July 2006.

Nelson, A.R., 1992, Lithofacies analysis of colluvial sediments – an aid in interpreting the recent history of Quaternary normal faults in the Basin and Range Province, western United States: Journal of Sedimentary Petrology, v. 62, p. 607-621.

Nelson, A.R., Lowe, M., Personius, S., Bradley, L.A., Forman, S.L., Klauk, R., and Garr, J., 2006, Paleoseismology of Utah, Volume 13 – Holocene earthquake history of the northern Weber segment of the Wasatch fault zone, Utah: Utah Geological Survey Miscellaneous Publication 05-8, 39 p., 2 plates.

Olig, S., McDonald, G., Black, B., DuRoss, C., and Lund, B., 2004, The Mapleton "Megatrench"; deciphering 11,000 years of earthquake history on the Wasatch fault near Provo: Utah Geological Survey, Survey Notes, v. 36, no. 2, p. 4-6, 8.

Ostenaa, D., 1984, Relationships affecting estimates of surface fault displacements based on scarp-derived colluvium deposits: Geological Society of America Abstracts with Programs, v. 16, no. 5, p. 327.

Puseman, K., 2005, Examination of bulk soil for radiocarbon datable material from the Santaquin fault trenches, Utah: Golden, Colorado, unpublished Paleo Research Institute Technical Report 05-58, 11 p.

Puseman, K., and Cummings, L.S., 2005, Separation and identification of charcoal and organics from bulk sediment samples for improved radiocarbon dating and stratigraphic correlations, *in* Lund, W.R., editor, Western States Seismic Policy Council Proceedings Volume of the Basin and Range Province Seismic Hazards Summit II: Utah Geological Survey Miscellaneous Publication 05-2, 10 p., compact disk.

Reimer, P.J., Baillie, M.G.L., Bard, E., Bayliss, A., Beck, J.W., Bertrand, C., Blackwell, P.G., Buck, C.E., Burr, G., Cutler, K.B., Damon, P.E., Edwards, R.L., Fairbanks, R.G., Friedrich, M., Guilderson, T.P., Hughen, K.A., Kromer, B., McCormac, F.G., Manning, S., Bronk Ramsey, C., Reimer, R.W., Remmele, S., Southon, J.R., Stuiver, M., Talamo, S., Taylor, F.W., van der Plicht, J., and Weyhenmeyer, C.E., 2004, IntCal04 terrestrial radiocarbon age calibration, 0-26 cal kyr BP: Radiocarbon, v. 46, no. 3, p. 1029-1058.

Schwartz, D.P., 2000, Recurrence of large earthquakes along the 1959 surface rupture at Hebgen Lake, Montana [abs]: Eos (Transactions of the American Geophysical Union), v. 81, no. 48, p. 1160-1161.

Schwartz, D.P., and Coppersmith, K.J., 1984, Fault behavior and characteristic earthquakes – examples from the Wasatch and San Andreas fault zones: Journal of Geophysical Research, v. 89, no. B7, p. 5681-5698.

Seitz, G.G., 1999, The paleoseismology of the southern San Andreas fault at Pitman Canyon – implications for fault behavior and paleoseismic methodology: Eugene, University of Oregon, Ph.D. dissertation, 278 p.

Slemmons, D.B., 1977, Faults and earthquake magnitude: U.S. Army Engineer Waterways Experiment Station, Vicksburg, Mississippi, Miscellaneous Paper S-73-1, Report 6, 129 p.

Solomon, B.J., Clark, D.L., and Machette, M.N., 2006, Interim geologic map of the Spanish Fork quadrangle, Utah County, Utah: Utah Geological Survey Open-File Report 488, 29 p., 1 plate, scale 1:24,000.

Stuiver, M., and Reimer, P.J., 1993, Extended ^{14}C database and revised CALIB radiocarbon calibration program: Radiocarbon, v. 35, p. 215-230.

Stuiver, M., Reimer, P.J., and Reimer, R., 2005, CALIB manual: Online, <http://calib.qub. ac.uk/calib/manual/>, accessed September 2006.

Swan, F.H., III, Schwartz, D.P., and Cluff, L.S., 1980, Recurrence of moderate to large magnitude earthquakes produced by surface faulting on the Wasatch fault zone, Utah: Bulletin of the Seismological Society of America, v. 70, no. 5, p. 1431-1462.

Tocher, D., 1958, Earthquake energy and ground breakage: Bulletin of the Seismological Society of America, v. 48, p. 147-153.

Wells, D.L., and Coppersmith, K.J., 1994, New empirical relationships among magnitude, rupture length, rupture width, rupture area, and surface displacement: Bulletin of the Seismological Society of America, v. 84, no. 4, p. 974-1002.

Witkind, I.J., and Weiss, M.P., 2002, Geologic map of the Nephi 30′ x 60′ quadrangle: Utah Geological Survey Map 189DM, 3 plates, scale 1:100,000.

Wong, I., Silva, W., Olig, S., Thomas, P., Wright, D., Ashland, F., Gregor, N., Pechmann, J., Dober, M., Christenson, G., and Gerth, R., 2002, Earthquake scenario and probabilistic ground shaking maps for the Salt Lake City, Utah, metropolitan area: Utah Geological Survey Miscellaneous Publication 02-5, 50 p.

APPENDIX

DESCRIPTION OF STRATIGRAPHIC UNITS IN SANTAQUIN TRENCHES AND TEST PIT

Trench 1, north wall															
Unit[1]	Genesis[2]	Texture[3]	Particle size distribution (%)[4]					Matrix color (dry)[5]	Datable organic materials and sample number	Structures[6]		Dry consistence[7]	Plasticity[8]	Other properties and comments[9]
			B	C	G	S	F			Depositional	Tectonic			
1	S	Sandy gravel with silt	0	<5	55	30	10	*10YR 6/4*	Gastropod shell fragments	Moderately to very well sorted; 10–30-cm-thick, west-dipping lenticular sand and gravel interbeds; mostly clast supported. Locally contains loess (50-cm-thick by 100-cm-long deposit) on fault footwall. Basal contact not exposed.	Faulted and fractured	Firm to hard	Low to medium	Mostly clast supported. Clasts: ang to subang, domin limestone, max 40 cm.
2	H	Silty gravel with sand	0	<5	50	25	20	*10YR 6/4*		Poorly to well sorted; fines up from silt, sand and gravel to bimodally distributed silt, sand, and cobbles. Minor, 10–20-cm-thick lenticular sand and gravel interbeds. Basal contact: 2–5 cm, wavy to irregular.	Faulted and fractured	Firm to hard	Low	Mixed clast and matrix supported. Clasts: ang to subang, domin quartzite, max 8 cm.
3	D	Silty gravel with sand and cobbles	0	5	40	25	30	*7.5YR 6/3-4*	Charcoal fragments (STRC-17, 18)	Poorly sorted (bimodally distributed); massively bedded, gravel with fines. Thin (5–10-cm-thick) coarse gravel at base. Basal contact: <2 cm, smooth.	Faulted and fractured	Hard to very hard	Medium	Mixed clast and matrix supported. Clasts: ang to subang, domin quartzite, max 53 cm.
4	D	Silty sand with gravel with and cobbles	<5	15	20	25	35	*7.5YR 6/3-5*		Poorly sorted (bimodally distributed); massively bedded, silt, sand, and gravel with randomly distributed cobbles. Basal contact: 2–5 cm, wavy.	Faulted and fractured	Hard to very hard	Medium	Mostly matrix supported, locally clast supported. Clasts: ang to subang, domin quartzite, max 30 cm.
5	S	Sandy gravel with silt	0	<5	60	25	10	*10YR 5/4*	Charcoal fragments (STRC-5, 7)	Moderately to very well sorted; 5–30-cm-thick lenticular silt, sand, and gravel interbeds common, with abrupt to gradational contacts. Locally poorly sorted (bimodally distributed). Basal contact: 2–5 cm, smooth to wavy.	Faulted and fractured	Firm to hard	Non plastic	Unit represents undivided unit 5. Mostly clast supported, locally matrix supported. Clasts: ang to subround, domin limestone and quartzite, max 28 cm.
5a	H	Silty gravel with sand and cobbles	0	5	60	25	10	*10YR 5/4*	Thin (<10-cm-thick) discontinuous, organic-rich laminations parallel to bedding. Charcoal fragments (STRC-9, 10)	Poorly to moderately sorted; laterally discontinuous – mostly limited to hanging wall of fault; may contain parallel gravel interbeds. Basal contact: 2–5 cm, smooth to wavy.	Faulted and fractured	Firm to hard	Non plastic	Mixed clast and matrix supported. Clasts: ang to subround, domin limestone and quartzite, max 13 cm.
5b	S	Sandy gravel with silt	0	<5	60	25	10	*10YR 5/4*	Charcoal fragments (STRC-8)	Moderately to very well sorted; 5–30-cm-thick lenticular silt, sand, and gravel interbeds common, with abrupt to gradational contacts. Locally poorly sorted (bimodally distributed). Basal contact: 2–5 cm, smooth to wavy.	Faulted and fractured	Firm to hard	Non plastic	Mostly clast supported, locally matrix supported. Clasts: ang to subround, domin limestone and quartzite, max 28 cm.
6	D	Silty gravel with sand and cobbles	0	15	25	20	40	*10YR 5/4*	Modern roots	Poorly sorted (bimodally distributed); massively bedded. Cobbles (15–20%) are randomly distributed. Fines dominantly silt. Basal contact: 2–5 cm, wavy.	Fractured	Hard	Medium	Matrix supported. Clasts: ang to subang, domin limestone, max 26 cm. Footwall exposure only; locally removed by unit 7.
7	H	Poorly graded gravel with cobbles	0	5	65	25	5	*10YR 5/3*	Some modern roots. Modern burrows and organic-rich fines in upper 10–20 cm (STBS-11, 16)	Poorly to moderately sorted; thin (5–10-cm-thick) fine gravel interbeds with cut and fill structure. Locally massively bedded. Basal contact: 2–5 cm, wavy to broken.	Faulted and fractured	Firm	Non plastic	Mixed clast and matrix supported. Clasts: ang to subang, domin quartzite, max 14 cm.
8a	C	Silty gravel with organic fines and sand	0	<5	60	25	10	*10YR 5/4*	Modern roots. Organic-rich matrix	Moderately sorted gravel with cobbles and slope-parallel fabric. May contain 5–10-cm-thick lenticular fine gravel interbeds dipping and tapering to northwest. Basal contact: 2–5 cm, wavy to irregular.	No evidence of deformation	Soft	Non plastic to low.	Mostly clast supported. Clasts: ang to subang, max 14 cm.
8b	C	Silty gravel with organic fines, sand, and cobbles	0	10	45	20	25	*10YR 3/4*	Modern roots. Organic-rich matrix	Moderately sorted gravel with cobbles, massively bedded. Basal contact: 5–10 cm, smooth to wavy.	No evidence of deformation	Firm	Medium	Mixed clast and matrix supported. Clasts: ang to subang, max 17 cm. Modern soil developed on unit. Soil: up to 12 cm thick, dark brown, organic-rich, root mixed.
9	D	Silty gravel with organic fines and cobbles	0	10	40	20	30	*10YR 4/4*	Modern roots. Organic-rich matrix (STBS-5)	Poorly sorted (bimodally distributed); massively bedded. Gravel/cobbles randomly distributed. Local massively bedded channels ~50 cm thick. Locally contains up to 20–30% cobbles. Basal contact 5–10 cm, wavy to irregular.	No evidence of deformation	Hard	Medium	Mostly matrix supported. Clasts: subang to subround, domin limestone and quartzite, max 50 cm. Soil developed on unit—up to 20 cm thick, dark brown, organic, root mixed.
10	D	Silty gravel with organic fines and cobbles	0	5	45	20	30	*10YR 4/4*	Modern roots. Organic-rich matrix	Poorly sorted (bimodally distributed); massively bedded. Gravel/cobbles randomly distributed. Local massively bedded channels 50–100 cm thick. Locally contains up to 10–20% cobbles. Basal contact 5–10 cm, wavy to irregular.	No evidence of deformation	Hard	Medium	Mostly matrix supported. Clasts: subang to subround, domin limestone and quartzite, max 22 cm. Soil developed on unit—up to 20 cm thick, dark brown, organic, root mixed.

Trench 2, south wall														
Unit[1]	Genesis[2]	Texture[3]	Particle size distribution (%)[4]					Matrix color (dry)[5]	Datable organic materials and sample number	Structures[6]		Dry consistence[7]	Plasticity[8]	Other properties and comments[9]
			B	C	G	S	F			Depositional	Tectonic			
1	S	Poorly graded sand with gravel and cobbles	0	5	35	55	5	*7.5YR 5/4*	2–15-cm-thick, discontinuous, organic-rich laminations parallel to bedding, charcoal fragments (STRC-13, 14)	Moderately to well sorted; 5–30-cm-thick, west-dipping lenticular sand and gravel interbeds; mostly clast supported. Basal contact not exposed.	Faulted and fractured	Soft to firm	Non plastic	Mostly clast supported. Clasts: ang to subang, domin limestone, max 24 cm.
2	S	Silty gravel with sand	0	<5	50	35	10	*10YR 5/6*		Moderately to well sorted; 5–20-cm-thick, west-dipping lenticular sand and gravel interbeds. Basal contact: 2–5 cm, wavy to irregular.	Faulted and fractured	Firm	Non plastic	Mostly clast supported. Clasts: ang to subang, domin limestone, max 17 cm.
3	H	Silty gravel with sand with cobbles	0	5	60	25	10	*10YR 6/6*		Poorly to moderately sorted; laterally continuous; may contain parallel gravel interbeds. Basal contact: 2–5 cm, wavy.	Faulted and fractured	Firm to hard	Low	Mixed clast and matrix supported. Clasts: ang to subang, domin limestone, max 20 cm.
4	S	Poorly graded gravel with cobbles	0	10	50	35	5	*10YR 5/8*	Some modern roots, rare charcoal fragments (STRC-15)	Package of 10–15-cm-thick, west-dipping sand and gravel interbeds, with parallel to lenticular, abrupt contacts. Basal contact: 2–5 cm, smooth to wavy.	Faulted and fractured.	Firm	Non plastic	Mostly clast supported. Clasts: ang to subround, domin limestone, max 17 cm.
5	D	Silty gravel with sand and cobbles	0	10	35	25	30	*10YR 5/4*	Charcoal fragments (STRC-1, 2)	Very poorly sorted (bimodally distributed), massive, consistent thickness. May contain fine-gravel interbeds; bedding locally indistinct. Basal contact: 2–5 cm, smooth to wavy.	Faulted and fractured	Hard	Medium	Matrix supported. Carbonate stringers common. Clasts: subang, max 15 cm.
6	H	Silty gravel with sand, cobbles, and boulders	5	15	40	20	20	*10YR 4/6*	Some modern roots	Poorly to well sorted (bimodally distributed). Basal contact: <2 cm, smooth to wavy.	Faulted and fractured	Firm	Low	Unit represents undivided unit 6 in fault zone. Mixed clast and matrix supported. Clasts: ang to subang, domin limestone.
6a	S	Silty gravel with sand	0	<5	45	40	10	*10YR 4/6*	Some modern roots	Moderately to well sorted; locally thin (5–20 cm) to medium (20–50 cm) bedded; laterally discontinuous on fault footwall. Basal contact: <2 cm, smooth to wavy.	Faulted and fractured	Firm	Non plastic	Mostly clast supported. Clasts: ang to subang, domin limestone, max 15 cm.
6b	H	Silty gravel with sand, cobbles, and boulders	5	15	40	20	20	*10YR 4/6*	Some modern roots. Modern burrows in upper 10–20 cm	Poorly to well sorted (bimodally distributed); laterally continuous; locally contains 10–20-cm-thick pea-gravel interbed. Basal contact: <2 cm, smooth to wavy.	Faulted and fractured	Firm	Low	Mixed clast and matrix supported. Clasts: ang to subang, domin limestone, max 34 cm.
7	D	Silty gravel with organic fines, sand, and cobbles	0	>5	40	20	35	*10YR 4/4*	Modern roots. Some modern burrows in upper 10 cm. A horizon (STBS-1, 2)	Poorly sorted (bimodally distributed). Organic fines with randomly distributed gravel clasts; locally cobble rich (5–10%). May contain ~5-cm-thick, discontinuous gravel interbeds at base. Basal contact: 5–10 cm, wavy to irregular.	Faulted and fractured	Firm to hard	Medium	Mostly matrix supported. Clasts: subang, domin limestone, max 21. A horizon development: 10–15-cm thick: dark brown, organic, root mixed.
8a	F	Silty gravel with organic fines, sand, and cobbles	0	>5	45	25	25	*10YR 4-5/4*	Modern roots. Organic-rich matrix (STBS-11)	Poorly sorted gravel with cobbles; massive. Matrix locally organic. Basal contact: 5–10 cm, wavy to irregular.	No evidence of deformation	Soft to firm	Low to medium	Mixed clast and matrix supported. Clasts: ang to subround, very loose, max 15 cm.
8b	C	Silty gravel with organic fines, sand, and cobbles	0	>5	45	25	25	*10YR 5/4*	Modern roots. Thin (2–5-cm-thick) discontinuous, west-dipping organic-rich laminations (STBS-9). Organic-rich matrix	Moderately sorted gravel with cobbles, fines upward and laterally (to east); slope-parallel clast fabric. Matrix locally very organic or absent. Basal contact: <2 cm, wavy to irregular, marked by cobble line.	No evidence of deformation	Soft to firm	Low to medium	Mostly clast supported, locally matrix supported. Clasts: ang to subround, very loose, max 22 cm. Wedge shaped.
8c	C	Silty gravel with organic fines	0	<5	40	20	35	*10YR 5/3*	Modern roots. Organic-rich matrix (STBS-10)	Moderately sorted gravel with cobbles, massively bedded; no grading. Gradually thickens downslope (to west). Basal contact: 2–5 cm, smooth to wavy.	No evidence of deformation	Soft	Medium	Mixed clast and matrix supported. Clasts: ang to subang, very loose, max 14 cm. Modern soil developed on unit. Soil: 10–15 cm thick, dark brown, organic-rich, root mixed.

Test pit, south wall														
Unit[1]	Genesis[2]	Texture[3]	Particle size distribution (%)[4]					Matrix color (dry)[5]	Datable organic materials and sample number	Structures[6]		Dry consistence[7]	Plasticity[8]	Other properties and comments[9]
			B	C	G	S	F			Depositional	Tectonic			
1	D	Silty gravel with organic fines and sand	0	<5	50	20	25	10YR 5/3	Organic fines concentrated within upper 10 cm of unit	Poorly sorted (bimodally distributed); locally moderately sorted fine gravel. Basal contact not exposed.	No evidence of deformation	Firm	Medium	Mostly matrix supported, locally clast supported. Clasts: subang, max 15 cm.
2	D	Silty gravel with organic fines, sand, and cobbles	0	5	45	25	25	10YR 4/4	Some modern roots. Organic-rich matrix (STBS-7)	Poorly sorted (bimodally distributed). Unit consists of a coarsening upward sequence. Basal contact: 2–5 cm, smooth to wavy.	No evidence of deformation	Firm	Low	Mixed clast and matrix supported. Clasts: subang to subround, max 28 cm.
3	D	Silty gravel with organic fines, sand, and cobbles	0	5	45	25	25	10YR 4/4	Some modern roots. Organic-rich matrix	Poorly sorted (bimodally distributed). Unit consists of a coarsening upward sequence. Basal contact: 2–5 cm, smooth to wavy.	No evidence of deformation	Firm	Low	Mixed clast and matrix supported. Clasts: subang to subround, max 17 cm.
4	D	Silty gravel with organic fines and sand	0	<5	40	25	30	10YR 4/3	Modern roots. Organic-rich matrix (STBS-6)	Poorly sorted (bimodally distributed); massively bedded. Randomly distributed gravel clasts with dark, organic fines. Local gravel interbeds at base. Basal contact: ~5 cm, wavy.	No evidence of deformation	Firm	Medium	Mostly matrix supported. Clasts: subang, max 10 cm. Modern A horizon: upper 10–15 cm of unit, dark brown, organic, root mixed.

[1] Units shown on the trench and test-pit logs (plate 1); differentiated based on lithology, stratigraphic position, and inferred genesis, inferred age; listed approximately from oldest to youngest.
[2] Inferred genesis; C – scarp-derived colluvium, D – debris flow, F – fissure fill, H – hyperconcentrated flow (mixed stream and debris-flow deposits; Giraud, 2005), S – stream/sheetwash deposits; two or more letters indicate multiple geneses, with first letter representing the dominant origin.
[3] Texture terms follow the Unified Soil Classification System. Textural information may not be representative of entire unit due to vertical and horizontal lithological heterogeneity in units.
[4] Percentage of clast-size fractions (based on area) are field estimates. B – boulders (>30 cm), C – cobbles (7.5–30 cm), G – gravel (0.2–7.5 cm), S – sand (0.074–2 mm), F – fines (silt and clay; <0.074 mm). We used a #10 sieve to separate clasts < 2 mmfrom gravel.
[5] Munsell color of matrix, taken dry.
[6] Terms follow Birkeland and others (1991).
[7] Dry consistence of matrix, based on ease/difficulty in breaking matrix by hand (Birkeland and others, 1991).
[8] Plasticity, based on rolling wet matrix between thumb and finger (Birkeland and others, 1991).
[9] Other properties may not be characteristic of entire unit. Abbreviations: ang – angular, domin – dominantly, max – maximum clast dimension, subang – subangular, subround – subrounded.

UTAH GEOLOGICAL SURVEY
a division of
UTAH DEPARTMENT OF NATURAL RESOURCES

Plate 1
Utah Geological Survey Special Study 124
Stratigraphic and Structural Relations in the Santaquin Fault Trenches and Test Pit, Nephi Segment

NORTH WALL OF TRENCH 1 AT THE SANTAQUIN TRENCH SITE

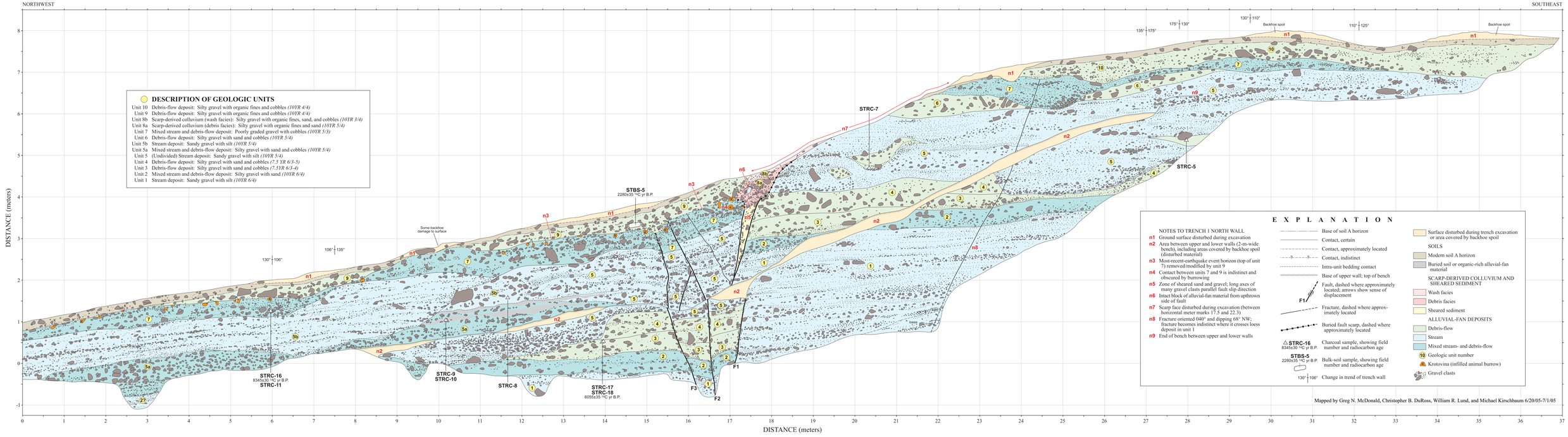

MIRROR IMAGE OF SOUTH WALL OF TRENCH 2 AT THE SANTAQUIN TRENCH SITE

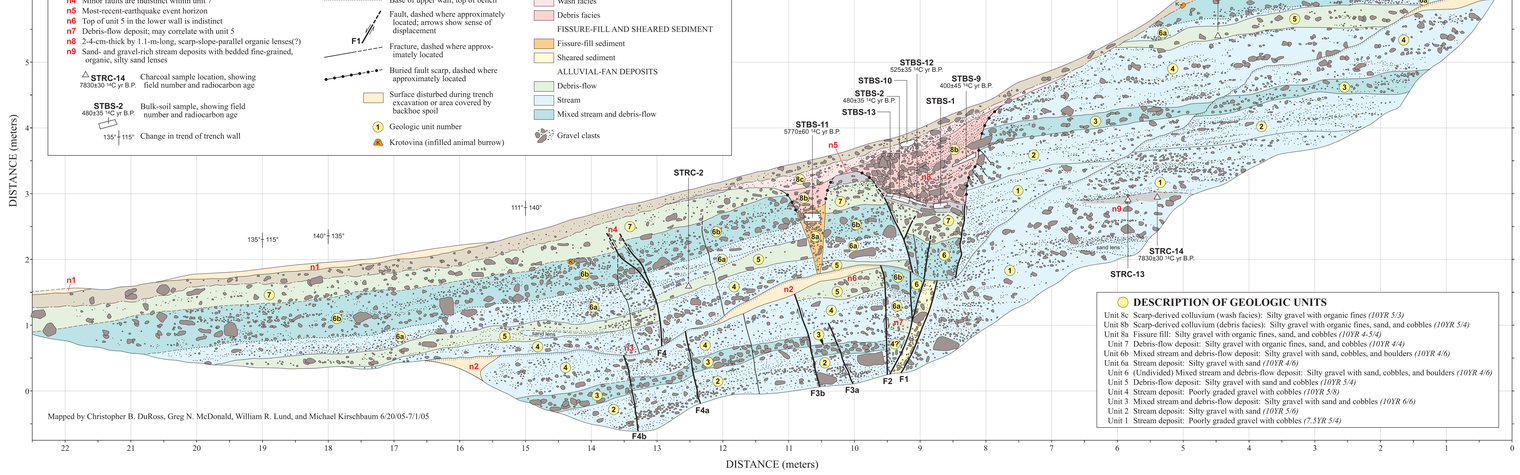

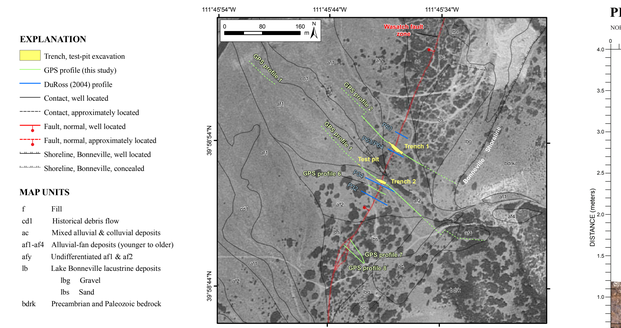

Location of Santaquin trenches, test pit, and scarp profiles. Dashed green lines indicate parts of profiles not shown on plate 1.

PHOTOMOSAIC OF NORTH WALL OF TRENCH 2 AT THE SANTAQUIN TRENCH SITE

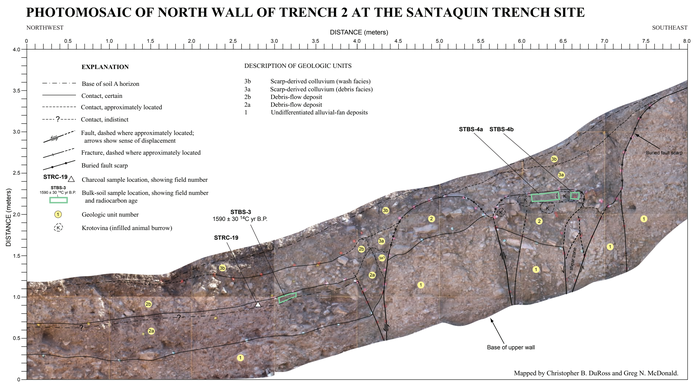

MIRROR IMAGE OF SOUTH WALL OF TEST PIT AT THE SANTAQUIN TRENCH SITE

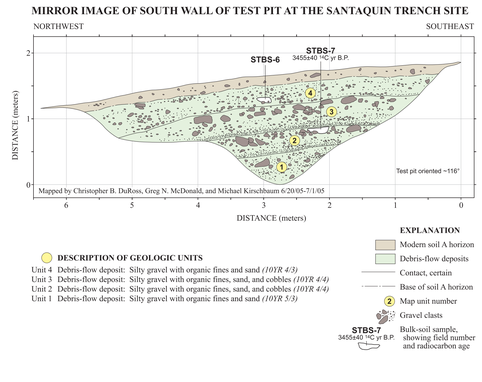

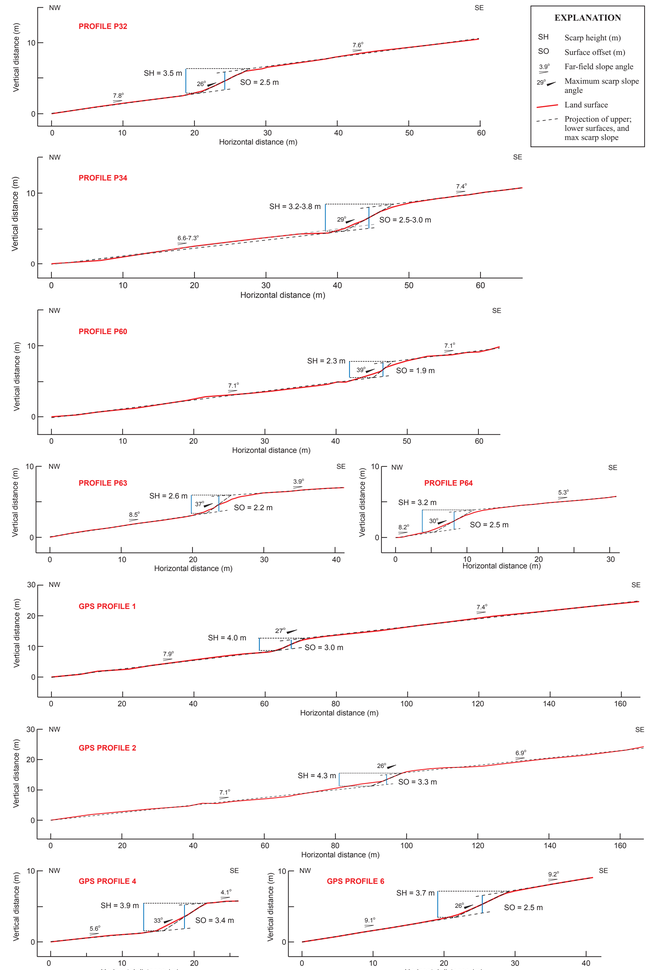

Fault-scarp profiles measured at the Santaquin trench site. GPS profiles 1, 2, 4, and 6 were measured using high-precision GPS equipment (this study). Profiles P32, P34, P60, P63, and P64 measured by DuRoss (2004). GPS profile 4 not shown on location map.

STRATIGRAPHIC AND STRUCTURAL RELATIONS IN THE SANTAQUIN FAULT TRENCHES AND TEST PIT, NEPHI SEGMENT, WASATCH FAULT ZONE

by Christopher B. DuRoss, Greg N. McDonald, and William R. Lund